Linking emissions of fossil fuel CO_2 and other anthropogenic trace gases using atmospheric $^{14}CO_2$

John B. Miller[1,2*], Scott J. Lehman[3*], Stephen A. Montzka[1], Colm Sweeney[1,2], Benjamin R. Miller[1,2], Anna Karion[1,2], Chad Wolak[3], Ed J. Dlugokencky[1], John Southon[4], Jocelyn C. Turnbull[1,2], Pieter P. Tans[1,2]

1. NOAA Earth System Research Laboratory, 325 Broadway, Boulder, CO 80305
2. Cooperative Institute for Research in Environmental Science, University of Colorado, Boulder CO 80309
3. Institute for Arctic and Alpine Research, University of Colorado, Boulder CO 80309
4. Department of Earth System Science, University of California, Irvine CA 92697

These authors contributed equally to the work

Abstract

Atmospheric CO_2 gradients are usually dominated by the signal from net terrestrial biological fluxes, despite the fact that fossil fuel combustion fluxes are larger in the annual mean. Here, we use a six year long series of $^{14}CO_2$ and CO_2 measurements obtained from vertical profiles at two northeast US aircraft sampling sites to partition lower troposphere CO_2 enhancements (and depletions) into terrestrial biological and fossil fuel components (C_{bio} and C_{ff}). Mean C_{ff} is 1.5 ppm, and 2.4 ppm when we consider only planetary boundary layer samples. However, we find that the contribution of C_{bio} to CO_2 enhancements is large throughout the year, and 60% in winter. Paired observations of C_{ff} and the lower troposphere enhancements (Δ_{gas}) of 22 other anthropogenic gases (CH_4, CO, halo- and, hydrocarbons and others) measured in the same samples are used to determine apparent emission ratios for each gas. We then scale these ratios by the well known US fossil fuel-CO_2 emissions to provide observationally-based estimates of national emissions for each gas and compare these to "bottom up" estimates from inventories.

Correlations of Δ_{gas} with C_{ff} for almost all gases are statistically significant with median r^2 for winter, summer and the entire year of 0.59, 0.45, and 0.42, respectively. Many gases exhibit statistically significant winter:summer differences in ratios that indicate seasonality of emissions or chemical destruction. The variability of ratios in a given season is not readily attributable to

meteorological or geographic variables and instead most likely reflects real, short-term spatio-temporal variability of emissions.

1. Introduction

Fossil fuel emissions have driven atmospheric CO_2 from about 280 ppm in the early 1800s to about 390 ppm presently, despite the uptake of about half of these emissions by the oceans and terrestrial biosphere [*Canadell et al.*, 2007; *Knorr*, 2009]. Although the recent CO_2 increase is clearly anthropogenic, individual atmospheric CO_2 observations are often dominated by seasonal and diurnal variability caused by the terrestrial biosphere. Thus, any attempt to determine fossil fuel emissions directly from local atmospheric observations requires the separation of fossil fuel and biospheric contributions to the measured CO_2 mole fraction. The ^{14}C content of CO_2 is an ideal tracer for this purpose [e.g., *Levin et al.,* 2003*; Levin and Karstens*, 2007; *Turnbull et al.*, 2006; *Turnbull et al.*, 2011b; *Vogel et al.*, 2010] since fossil fuel-derived CO_2 is free of ^{14}C while all other significant sources have ^{14}C:C ratios close to that of the atmosphere. Over large industrialized land areas such as Eurasia and North America, the use of ^{14}C to isolate the recently-added fossil fuel contribution also quantifies (by difference) the change in atmospheric CO_2 due to uptake and release by the terrestrial biosphere [e.g., *Turnbull et al.*, 2006].

The global atmospheric CO_2 increase and global fossil fuel emissions are the best known components of the global carbon budget. Fossil fuel emissions are typically calculated from economic statistics on fuel production and/or consumption, for which good records exist in many countries [*Gregg et al.*, 2009]. At the global scale, uncertainty in annual emissions is estimated to be ~5% [*Marland*, 2008]. Uncertainties are larger and more difficult to characterize at regional spatial scales (~ 10^6 km^2) and for most individual countries. Moving from annual to monthly time scales can also greatly increase uncertainty. However, for the United States (US), accurate constraints on fuel sales exist at the state and monthly levels [*Gregg et al.*, 2009]. Thus, US totals aggregated at the annual and national scale or the state and monthly scale are most likely reliable to within ~10%.

Ultimately, it will be desirable to estimate emissions of fossil fuel derived CO_2 and other greenhouse gases with quantitative uncertainties, both within the US and internationally, based directly on atmospheric observations, as a means of evaluating compliance with regional emissions targets and international treaty obligations. A recent model experiment conducted at NOAA/ESRL suggests that the deployment of 5,000 to 10,000 paired ^{14}C and CO_2 measurements per year could provide an independent constraint on US national emissions with an estimated monthly uncertainty of ~10% at a spatial scale of ~$5x10^5$ km^2 (i.e., about the area of California). This strategy of emissions verification has been recommended by the National Research Council [*Committee on Methods for Estimating Greenhouse Gas Emissions*, 2010] but has not yet been implemented at the necessary scale. In the meantime, more modest measurement programs, like that described in this study, have several valuable near-term applications.

Here we pursue one such application, which takes advantage of the relatively high accuracy of fossil fuel emissions inventories in the US, the fact that $^{14}CO_2$ provides a reliable tracer for these emissions, and that $^{14}CO_2$ measurements made within the NOAA/ESRL air sampling network are paired with measurements of CO_2, CO, CH_4, N_2O, and SF_6, and a large suite of halo- and hydro-carbons. This permits us to scale emissions of these correlate gases to those for fossil fuel CO_2, providing in some instances the first "top down", observationally-based emissions estimates of these gases, many which influence climate, air quality and stratospheric ozone. Eventually, the same correlations may also permit the development of empirically-derived, proxy tracers of fossil fuel CO_2, as has been attempted previously using correlations of fossil fuel-derived CO_2 and CO [*Turnbull et al.*, 2011b; *Vogel et al.*, 2010].

Our results are based on a six-year time series of, typically, fortnightly $^{14}CO_2$, CO_2 and anthropogenic trace gas measurements from airborne sampling profiles downwind of the northeastern US, a region of significant anthropogenic emissions in North America. The ^{14}C and CO_2 measurements are used to determine the enhancements of fossil fuel-CO_2 below 2600 m asl with respect to the overlying free troposphere sampled in the same profile. We define this lower troposphere (often Planetary Boundary Layer, or PBL) enhancement as "C_{ff}". We then calculate ratios between lower troposphere enhancements of other anthropogenic trace gases and C_{ff} measured in the same profile, which we define as "apparent" emissions ratios since they are emissions ratios apparent at the time of observation as opposed to time of emission.

This method reveals statistically significant correlations between a wide range of anthropogenic gases and C_{ff} in summer, winter, and year-round. In contrast, summertime correlations of trace gas enhancements with the PBL enhancement or depletion in total CO_2 do not exist in summer, due to added variability imposed on the CO_2 signal by exchange with the terrestrial biosphere. We also find that in winter, when statistically significant correlations of trace gas enhancements and observed CO_2 enhancement do exist, they are, on average, biased by about a factor of two due to contributions from biospheric respiration. The finding of statistically significant correlations between enhancements of various anthropogenic gases and C_{ff} leads us to explore their use in determining trace gas emissions and their related uncertainties.

Below, we first present the isotope systematics and analytical framework that underlie our C_{ff} detection algorithm and describe our sampling and measurement methods. This is followed by a presentation of the primary results, including decomposition of the observed CO_2 signal into its fossil fuel and biological components and determination of trace gas enhancement:C_{ff} ratios, correlation coefficients and ratio distributions. We then discuss the apparent emissions ratios and their transformation to "absolute" emissions on a gas-by-gas basis, including a comparison to available "bottom up" inventories. Finally, we evaluate the potential uncertainties, biases and limitations of our methods.

2. Methods

2.1. Isotope systematics and data analysis

"Fossil" fuels are, by definition, devoid of ^{14}C because the half-life of ^{14}C is 5700±30 years [National Nuclear Data Center, Brookhaven National Laboratory, www.nndc.bnl.gov], while these fuels are typically hundreds of millions of years old. In contrast, the other significant sources of CO_2 to the atmosphere bear ^{14}C: C signatures that are near equilibrium with the atmosphere. In simplified form, $\Delta^{14}C \approx [(^{14}C/C)_{sample}/(^{14}C/C)_{standard}-1]1000‰$ but with corrections for mass-dependent fractionation (from in line $\delta^{13}C$ measurement) and small amounts of radioactive decay between the times of sampling and measurement [see Stuiver and Pollach 1977 for full expression]. Thus, ^{14}C-free fossil fuel-CO_2 has a "delta" value of -1000 ‰. In contrast, the atmosphere during our measurement period has averaged about +50 ‰. By mass balance, the addition of 1 ppm of fossil CO_2 to an atmospheric burden of 390 ppm will produce a $\Delta^{14}C$ depletion of 2.7 ‰ (i.e. (-1000-50)/390).

The global atmospheric budgets for CO_2 and its $^{14}C:C$ ratio (expressed in the Δ notation and following $^{13}CO_2$ budget [*Tans et al.*, 1993]) are shown below in equations 1a and b;

$$\frac{dC_{atm}}{dt} = F_{bio} + F_{oce} + F_{fos} \tag{1a}$$

$$C_{atm}\frac{d\Delta_{atm}}{dt} = (\Delta_{fos} - \Delta_{atm})F_{fos} + \Delta_{ocedis}F_{ocedis} + \Delta_{biodis}F_{biodis} + isoF_{nuc} + isoF_{cosmo} \tag{1b}$$

C_{atm} refers to the atmospheric mole fraction of CO_2 and Δ_{atm} to its isotopic ratio. F_x refers to the flux of a given budget term into the atmosphere. The subscript "bio" represents the net terrestrial biosphere-atmosphere flux, "oce" is the net ocean-atmosphere flux, and "fos" is the flux from fossil fuel combustion. For the isotopic mass balance, Δ_x refers to the isotopic signature associated with a given flux. The subscript "ocedis" represents the ocean-atmosphere isotopic disequilibrium and "biodis" refers to the biosphere-atmosphere isotopic disequilibrium. Isotopic disequilibrium refers to the difference between isotopic signatures of carbon leaving and entering a reservoir, and the disequilibrium terms are therefore scaled by gross fluxes (not net fluxes as in eq. 1a). In the terrestrial case, disequilibrium results from the respiration of ^{14}C-enriched CO_2 photosynthetically assimilated when the atmospheric $\Delta^{14}C$ was much higher, primarily as a result of atmospheric nuclear weapons testing. In the oceanic case it results from the reemergence of ^{14}C-depleted CO_2 in surface waters, which have been out of contact with the atmosphere long enough for radioactive decay to become significant. The subscript "nuc" refers to the flux of $^{14}CO_2$ from nuclear reactors, and "cosmo" to the cosmogenic production of ^{14}C. These last terms are pure ^{14}C fluxes and as such don't have isotopic signatures and are represented only as "isoflux" terms, '$isoF_x$'. The cosmogenic ^{14}C production and subsequent oxidation to $^{14}CO_2$ both occur mainly in the stratosphere, from where the new $^{14}CO_2$ is mixed into the troposphere [*Naegler and Levin*, 2006; *Randerson et al.*, 2002; *Turnbull et al.*, 2009]. Note that whereas the net ocean and biosphere flux terms are important for the CO_2 budget, they do not appear in the isotopic mass balance. This is because the Δ notation includes a ^{13}C:^{12}C normalization that accounts for all sources of mass-dependent fractionation, including photosynthesis and net ocean exchange [*Stuiver and Pollach,* 1977]. If the non-fossil terms in the isotopic budget are either small or uniform in spatial distribution, then the theoretical mass-balance sensitivity and the associated measurement uncertainty will closely approximate the actual fossil fuel CO_2 detection capability.

To illustrate this, we show in Figure 1 a map of wintertime PBL (~ 300 m asl) fossil fuel-derived CO_2 and (total) $\Delta^{14}CO_2$ over eastern North America as represented in the TM5 transport model [*Krol et al.*, 2005], using a similar specification of budget terms as in Turnbull *et al.* [2009], but with no "tuning" to ensure global mass balance. For $^{14}CO_2$, all terms in eq. 1b are represented in the model, except the nuclear term [*Graven and Gruber*, 2011]. The color scales depicting $\Delta^{14}CO_2$ and fossil fuel CO_2 distributions correspond to the expected mass balance sensitivity of -2.7 ‰/ppm. Thus, the similar colors and patterns in Figure 1 indicate that, over eastern North America, the ^{14}C horizontal and vertical (not shown) gradients are controlled largely by the presence of fossil fuel CO_2. The remaining small differences are due primarily to small atmospheric gradients imposed by the terrestrial disequilibrium flux of ^{14}C ($\Delta_{biodis}F_{biodis}$ in eq. 1b). This contribution can be quantified and applied as a small correction in the fossil fuel CO_2 detection algorithm, as discussed below. ^{14}C emissions from nuclear power generation [*Graven and Gruber*, 2011], which are neglected in the TM5 simulations due to large relative uncertainty, may produce near-surface signals averaging 1 to 2 ‰ in the densely populated northeastern US as discussed in *Section 4.6.2*. The cosmogenic production and ocean disequilibrium terms, which are important globally, do not result in significant simulated gradients of ^{14}C over the US.

In order to quantify the fossil fuel CO_2 signal from measurements, we follow Levin *et al.* [2003] in considering observations of both CO_2 and $\Delta^{14}C$ to be the sum of background values for each tracer plus any fossil fuel and biospheric contributions;

$$C_{obs} = C_{bg} + C_{ff} + C_{bio} \qquad (2a)$$

$$\Delta_{obs}C_{obs} = \Delta_{bg}C_{bg} + \Delta_{ff}C_{ff} + \Delta_{bio}C_{bio} \qquad (2b).$$

As in Turnbull *et al.* [2006], we divide C_{bio} into photosynthetic and respiratory terms C_{photo} and C_{resp}, respectively. Expanding and combining eqs. 2a and b, and setting Δ_{photo} equal to Δ_{bg} (which will be the same as a result of ^{13}C:^{12}C normalization), we obtain

$$C_{ff} = \frac{C_{obs}(\Delta_{obs} - \Delta_{bg})}{\Delta_{ff} - \Delta_{bg}} - \frac{C_{resp}(\Delta_{resp} - \Delta_{bg})}{\Delta_{ff} - \Delta_{bg}} \quad (2c).$$

In eq. 2c, all of the quantities in the first term on the right-hand-side are either known *a priori* or can be measured, and the second term, which we call C_{corr}, is a correction to C_{ff}, which accounts for the disequilibrium contribution of ^{14}C from heterotrophic respiration. The recent isotopic disequilibrium is approximately [*Ciais et al.*, 1999] the difference between present day atmospheric $\Delta^{14}C$ and that from a decade or so earlier, reflecting the mean residence time of carbon in the terrestrial biosphere. C_{corr} was estimated previously as 0.4 - 0.8 ppm in summer and 0.2 – 0.3 ppm in winter, based on the seasonally varying heterotrophic respiration flux and PBL height and the mean terrestrial biosphere isotopic disequilibrium [*Turnbull et al.*, 2009; *Turnbull et al.*, 2006].

For this study, we calculate C_{corr} explicitly for each lower troposphere sample. To do this we use the FLEXPART Lagrangian particle dispersion model [*Stohl et al.*, 2005; see also *Section 2.4*] in backwards mode and driven by NCEP Global Forecast System 1˚ x 1˚ winds to produce seven-day surface influence functions for each sample. We use impulse-response functions generated from the CASA biogeochemical model [*Thompson and Randerson*, 1999] to estimate the age distribution of heterotrophic respiration at each 1˚x1˚ terrestrial grid cell for each month and convolve this with the atmospheric history of $\Delta^{14}C$ to yield the factor Δ_{biodis} [cf., *Randerson et al.*, 2002]. F_{biodis} is also calculated at monthly, 1˚x1˚ resolution from the same CASA response functions. The integrated surface sensitivity derived from FLEXPART for a given lower troposphere air sample (in units of [ppm/(μmol $m^{-2}s^{-1}$)]) is multiplied by the disequilibrium flux ($\Delta_{biodis}F_{biodis}$, in units of [μmol $m^{-2}s^{-1}$ ‰]) for the same seven-day period preceding the sample time, and summed over all grid cells. This yields the numerator of C_{corr}. Sample-by-sample C_{corr} values for one of our measurements sites (CMA in Fig. 1 and *Section 2.2*) are shown in Figure 2. C_{corr} for samples obtained from above or near the top of the PBL is small relative to near-surface values in both winter and summer as a result of diminished sensitivity to the surface disequilibrium flux, and is near zero in winter when samples are (according to FLEXPART) above the wintertime PBL. Our C_{corr} values are consistent with the earlier seasonal estimates for the lower PBL but allow us to account for short-term variability in the correction on a sample-by-sample basis. The sensitivity of C_{ff} to C_{corr} is discussed in *Section 4.6.2.* Having estimated C_{corr}, the C_{ff} enhancement relative to background is calculated from eq. 2c. Equation 2a can then be applied to isolate C_{bio}, which is the biological enhancement or depletion of CO_2 relative to background.

In the present study our observations come from airborne, vertical sampling profiles, as described in *Section 2.2*. Thus, we apply eqs. 2a-c in a one-dimensional (1-D) vertical sense and assume that the free troposphere is the source of air into which fluxes of CO_2 and other gases are added in the PBL. Specifically, C_{bg} and Δ_{bg} are represented by paired CO_2 and $\Delta^{14}CO_2$ measurements from the free troposphere, and C_{obs} and Δ_{obs} are represented by lower-altitude (usually PBL) measurement pairs in the same profile. This is equivalent to stating that the chemical composition of the free troposphere is the same as the boundary layer air was several days in the past, prior to significant recent contributions from the surface. Although we are not calculating fluxes using vertical gradients, the 1-D assumption of the free troposphere as the appropriate background for the PBL is similar to that of most boundary layer budgeting approaches [e.g., *Bakwin et al.*, 2004; *Helliker et al.*, 2004; *Lloyd et al.*, 2001; *Lloyd et al.*, 2007]. An important example of when this assumption will not hold would be during the summer on the NE US coast where surface air may originate from the southwest, while free troposphere air may originate from the west. In the *Discussion* (*Section 4*), we will examine the extent to which the assumptions in our analysis might affect our interpretations. Here we simply note that the 1-D framework we apply provides a relatively straightforward interpretation of results, permitting us to focus on the observations themselves rather than on the analysis and discussion of the potential biases of individual atmospheric transport models.

We correlate C_{ff} with enhancements of other anthropogenic tracers determined in the same air samples in which CO_2 and $\Delta^{14}C$ are also measured. The enhancement for a given tracer is Δ_{gas}, and the apparent emissions ratio, R_{gas} is:

$$R_{gas} = \frac{X_{obs} - X_{bg}}{C_{ff}} = \frac{\Delta_{gas}}{C_{ff}} \qquad \text{(eq. 3)}$$

As with eq. 2a, “obs” refers to lower troposphere (usually PBL) samples and “bg” to those from the free troposphere. The gases to which we correlate C_{ff} are listed in Table 1 and include CH_4, N_2O, CO, SF_6, and a number of CFCs, HCFCs, HFCs, chlorinated solvents and hydrocarbons. For comparison, we also correlate Δ_{gas} with total CO_2 enhancement, C_{tot}, where $C_{tot} = C_{ff} + C_{bio} = C_{obs}\text{-}C_{bg}$.

2.2 Air Sampling

Air samples were collected aboard light aircraft flying above the ocean, downwind of the U.S. northeast Atlantic (Fig. 1). Lower troposphere (< 2600 m asl) samples are typically collected in the late morning. Observations at NHA began in 2004 and in 2005 at CMA and extend to the end of 2009, with a sampling frequency averaging twice per month at both sites. NHA (42.95 N, 70.63 E) is about 75 km NNE of Boston, and CMA (38.83˚N 74.32˚W) is about 235 km E of Washington DC. At both sites, 12 samples are collected semi-automatically using a programmable flask package (PFP; version 3) in which the pilot initiates sampling at pre-determined altitudes using a remote control. Samples are pressurized to 260 kPa in 0.7 L boro-silicate flasks. Full details of the sites and flask collection method are described at www.esrl.noaa.gov/gmd/ccgg/aircraft/. Our high precision $\Delta^{14}C$ analysis presently requires ~2 standard liters of air yielding, at ambient CO_2 levels, ~0.5 mg C. Only ~0.5 L of air remains in an individual flask after analysis of other gases. Thus, at three altitudes a second air sample dedicated to $\Delta^{14}C$ is collected for combination with residual air in the first sample. Figure 3 shows examples of vertical profiles from CMA from Feb. 21, 2007 and NHA from July 10, 2008. The full suite of measurements is available for 9 levels and $\Delta^{14}C$ is available for 3 prescribed levels, nominally 300 meters above sea level (m asl), 2100 m asl and 4000 m asl, based on aircraft pressure-altitudes. The sampling protocol at NHA is the same, but on alternate weeks the altitude of the middle $\Delta^{14}C$ sample is approximately 2400 m asl instead of 2100 m asl. In addition, a few of the earliest upper level $\Delta^{14}C$ measurements at NHA were higher than 4000 m asl. Data are available via anonymous FTP at ftp://ftp.cmdl.noaa.gov/ccg/co2c14/flask/. Over the continent the PBL height tends to be lower in winter. As a result, the mid-altitude levels will frequently be outside the PBL. $\Delta^{14}C$ sampling at these levels was implemented to provide an eventual constraint on the venting of fossil fuel CO_2 emissions through the top of the PBL, but this is not the focus of the present study.

2.3. Measurement

After sampling, all PFPs are sent to NOAA/ESRL where they undergo measurement for the trace gases in Table 1. Isotopic measurements are performed at the University of Colorado, Institute for Arctic and Alpine Research (INSTAAR). Details of $\Delta^{14}C$ analysis are similar to those presented by Turnbull *et al.* [2007]. Briefly, for $\Delta^{14}C$ analysis, CO_2 in the air samples is quantitatively extracted cryogenically. The pure CO_2 is then reduced to elemental graphite over a Fe catalyst in the presence of H_2. Extraction, graphitization, and pressing of the graphite into target cartridges occur at the INSTAAR Laboratory for AMS Radiocarbon Preparation and Research (NSRL). Graphite targets, typically containing about 0.5 mg C, are then analyzed by accelerator mass spectrometry (AMS) at the University of California, Irvine Keck Carbon Cycle AMS Facility using high-count, high-precision protocols developed for C_{ff} detection. Primary and secondary measurement standards and process blanks (^{14}C-dead CO_2 in air) are prepared at NSRL and measured alongside authentic samples. Measurement uncertainties (formally, measurement "repeatability" [*JCGM*, 2008]) are assessed by long-term repeated analysis of aliquots of whole air from high-pressure "surveillance" cylinders having $\Delta^{14}CO_2$ close to that of the ambient atmosphere. The extraction procedure is the same as for authentic flask samples, and there is no discernable bias between flask and cylinder extraction as verified by filling flasks from high-pressure cylinders. The pooled mean 1-sigma repeatability for three different surveillance cylinders used during the period of this study is 1.8 per mil and there is no evidence of drift in the mean values over time. Reported uncertainties are the larger of the long-term 1-sigma repeatability or the 1-sigma single-sample measurement uncertainty. ^{14}C measurement errors dominate the overall uncertainty of the C_{ff} in eq. 2c. The average one-sigma uncertainty of C_{ff} (and, thus, C_{bio}) is 1 ppm and is estimated by propagating analytical uncertainties of 1.8 per mil ($\Delta^{14}C$) and 0.1 ppm (CO_2) through eqs. 2a-c.

Halocarbon and non-methane hydrocarbon analyses were performed by gas chromatograph/mass spectrometry (GC/MS) [*Montzka et al.*, 1993], using either of two instruments. One approximately 200 cc (STP) aliquot was extracted from each PFP flask, pre-concentrated cryogenically on uncoated 0.53 mm I.D. fused silica tubing at ~ -170°C, then desorbed onto either a 60m DB-5 or a combined 25m DB-5 plus 30m GasPro capillary column for subsequent chromatographic separation with temperature-ramping in an Agilent 5890 or 6890 GC, and finally detection by an Agilent 5971 or 5973 quadrapole MS. Sample responses were determined relative to compressed whole air (Niwot Ridge, Colorado) reference gases, which were in turn assigned absolute calibration by comparison with primary standards prepared with gravimetric techniques at NOAA/ESRL. Analytical methods for the remaining gases are described at www.esrl.noaa.gov/gmd/ccgg/aircraft/ and analytical uncertainties for all gases are presented in Table 1.

2.4. Lagrangian atmospheric transport modeling

The FLEXPART Lagrangian particle dispersion model [*Stohl et al.*, 2005] was used both to determine C_{corr} for individual observations and for analysis of variability in our results not readily explained by our 1-D analytical framework. The model calculated back trajectories for ensembles of 10,000 randomly perturbed particles from the time and place of our measurements in order to trace the history of the air masses we have sampled. FLEXPART was forced with NCEP Global Forecast System 1˚ x 1˚ winds taken from the analysis and 3-hour forecast steps of the NCEP operational model, and mixing resulting from convection and PBL diffusion is parameterized. Back trajectories are run seven days back in time with output collected at 3-hour intervals. The model uses the intersection of particle back-trajectories with a 100 m layer of air above the surface to calculate "footprints". Footprints quantify the sensitivity of mole fraction changes at the air sampling location to upwind sources and sinks, as function of both space and time.

3. Results

In order to characterize CO_2 and anthropogenic trace gas signals in the NE US we begin by combining observations for the two sites and consider differences by altitude, using a dividing altitude of 2600 m asl (Fig. 4), which ensures that only the 4 km asl samples define background. In *Section 4.3* we examine possible contributions to variability in the observations that may be due to combining data from two different locations.

Analysis of the combined higher altitude (~ 4000 m asl) CO_2 time series shows the expected first-order behavior, with winter maxima and summer minima reflecting net respiration and net photosynthesis, respectively, of the terrestrial biosphere. The lower altitude time series is qualitatively similar but exhibits a greater range and more variability, with an average seasonal amplitude of 16 ppm compared to 10 ppm aloft. Additionally, the lower altitude seasonal cycle leads the seasonal cycle in the high altitude observations by 43±3 days. This lag is consistent with an immediate influence of CO_2 sources and sinks on the composition of the PBL and a delay, corresponding to timescales of vertical and horizontal mixing, in the response of the free troposphere. Signal amplitude and phase were determined using methods of Thoning *et al.* [1989].

The high and low altitude $\Delta^{14}C$ time series contrast markedly with those for CO_2 (Figure 4). The high altitude $\Delta^{14}C$ time series has a weak seasonal cycle that is not obviously in phase with that for CO_2. The most prominent feature of the series is the near-linear secular decline that reflects the dominant role of fossil fuel CO_2 emissions in the current global $\Delta^{14}C$ budget (eq. 1b) [*Naegler and Levin*, 2006; *Turnbull et al.*, 2009]. The lower altitude time series is almost uniformly lower in $\Delta^{14}C$ than the high altitude one, indicating the addition of ^{14}C-free fossil fuel CO_2 into the PBL. As with CO_2, the low altitude $\Delta^{14}C$ time series is more variable than the high altitude series due to the relative proximity to surface sources. With the exception of the long-term trends, which in each case result from the ongoing addition of fossil fuel CO_2 to the atmosphere, the information content of the CO_2 and $\Delta^{14}C$ time series is largely independent and complementary.

Applying eqs. 2a-c to the $\Delta^{14}C$ and CO_2 measurements from individual aircraft profiles, we estimate the fossil (C_{ff}) and biogenic (C_{bio}) CO_2 contributions for each observation in the lower altitude CO_2 time series. These are shown along with the difference in total CO_2 (C_{tot}) between higher- and lower- altitude measurements in Figure 4c. C_{ff} ranges between +13 and -3 ppm. Negative instances of C_{ff} are not physically realistic and comprise 18% of all observations (Fig. 4d). 15% of negative C_{ff} values originate from differences between the mid- and high- altitude samples, which are frequently both outside the PBL. Only 7% of the low altitude C_{ff} values are negative, which can be fully explained by the C_{ff} uncertainty of ± 1.0 ppm. The mean C_{ff} for all low altitude samples is 2.4 ± 2.2 ppm (one sigma).

The histogram of C_{bio} distributions (Fig. 4d) indicates that C_{bio} is evenly distributed over both positive and negative values as is expected based on the known seasonal flux dynamics of CO_2. It is important to note that in the absence of $\Delta^{14}C$ measurements, reliable partitioning of C_{tot} into C_{ff} and C_{bio} is not possible [cf. *Turnbull et al.*, 2006]. Thus, summertime drawdown of CO_2 would be underestimated (i.e. masked by C_{ff} as in Fig. 3b) and wintertime biospheric release of CO_2 overestimated (i.e. augmented by C_{ff} as in Fig. 3a) using only C_{tot} (Fig. 4c).

High and low altitude time series for the suite of other anthropogenic tracers show qualitatively similar behavior to $\Delta^{14}C$, with low variability at altitude and greater variability and enhancement closer to the surface (Fig. 5). CO, CH_4, CH_2Cl_2, benzene and other hydrocarbons all have seasonal cycles with summertime minima, most likely as a result of greatly enhanced summertime destruction by OH (Table 2). Many gases, including SF_6, N_2O, HFCs and HCFCs display noticeable concentration increases over time due to continued and in some cases increasing emissions [*Dlugokencky et al.*, 2009; *Montzka et al.*, 2011].

Figures 6a and b show scatter plots of C_{tot} or C_{ff} versus Δ_{gas} for the other measured anthropogenic gases in the same profile samples. Uncertainties for Δ_{gas} are derived from the respective analytical uncertainties (Table 1), where $\sigma_{dif} = \sigma_{analytical}\sqrt{2}$, and are plotted as error bars when they exceed the symbol size. Statistically significant correlations (expressed as r^2 values, $p<0.05$) are given for winter (November through February), summer (May through September), and for the entire year. Correlations with

C_{tot} tend to be strong in winter, but are weak or absent in summer. In contrast, statistically significant and generally strong correlations with C_{ff} are observed during both winter and summer for all species, although the wintertime correlation coefficients with C_{ff} are generally lower than for those with C_{tot}. Year-round correlations with C_{ff} are still significant but tend to be weaker than either the summer or winter correlations alone, especially for gases that appear to exhibit seasonal variations with respect to C_{ff}.

The statistically significant correlations we observe (Table 1, Fig. 6b) link C_{ff} to enhancements of a wide variety of anthropogenic compounds. Although only CO, NMHCs and CH_4 are potentially co-emitted with CO_2 during fossil fuel combustion, other tracers also show statistically significant correlations with C_{ff}. This is most likely because our observation sites lie hundreds of km downwind of large urban/suburban anthropogenic emission sources. At this length scale, atmospheric mixing appears to homogenize tracers of a variety of anthropogenic emissions so as to produce statistically significant signals even though their sources are not precisely co-located.

We calculate apparent emission ratios, R_{gas}, on a sample-by-sample basis (eq. 3) and show the time series and seasonal distributions of R_{gas} in Figure 7. The presence of statistically significant seasonal differences in R_{gas} is shown in Table 2. The uncertainty of ratios for individual samples is propagated from the uncertainties previously calculated for C_{ff} and Δ_{gas}. For the sample-by-sample analysis, we filter the ratios to remove those with relative uncertainty greater than 100% at the one-sigma level. This is nearly identical to filtering based only on uncertainty in C_{ff}, because C_{ff} uncertainty dominates the uncertainty for all ratios except SF_6 and N_2O.

For gases other than non-methane hydrocarbons (NMHCs), the highest ratios tend to occur in summer. But the summertime populations also include lower ratios that are characteristic of winter, indicating greater variability of ratios during summer. For the NMHCs, higher ratios tend to occur in winter as a result of enhanced consumption by OH in summer. In almost all cases the seasonal distributions of ratios as shown by the histograms are broad and skewed. The skew arises in part because actual (as opposed to apparent) emissions ratios must be positive.

Negative apparent emissions ratios (below the 1 sigma threshold) occur most commonly in summer (Fig. 7) and for gases with lifetimes with respect to OH less than one year (Table 2). These ratios generally reflect times when the low- and/or mid-level mole fraction of a given gas (CO, C_2H_2, etc.) is depleted relative to that measured in the free troposphere, and only rarely instances when the expected $^{14}CO_2$ vertical difference is "reversed". In *Section 4.2.1* we discuss the possible causes of negative ratios.

The largely non-Gaussian distributions of sample-by-sample emissions ratios (Fig. 7) indicate that seasonal or year-round emissions cannot be adequately characterized by a single metric such as a regression slope or arithmetic mean and standard deviation. In *Section 4.2* we describe the year-round and seasonal emissions ratios and test for seasonality of emissions based on the distributions of ratios for each gas. We also address the extent to which the widths of the distributions may reflect "noise" resulting from possible shortcomings of our 1-D analytical framework, real variations in the actual emission ratios over space and time, and variances arising from physical separation of different types of fossil fuel CO_2 emissions.

4. Discussion

4.1 Observational bias in C_{tot} from C_{bio}

Our results show strong correlations between many trace gases and total CO_2 enhancements during winter (average Δ_{gas}:C_{tot} $r^2 = 0.60$) despite large contributions of C_{bio} to C_{tot}. Excluding negative instances of C_{ff} (non-physical) and negative instances of C_{bio} (apparent wintertime uptake), the mean wintertime C_{bio} we calculate is 3.5±2.6 ppm and the mean fraction of the total wintertime CO_2 enhancement originating from the terrestrial biosphere is 58 ± 22%. Note that the standard deviation of the fraction is much lower than that for either C_{bio} or C_{tot} alone, because C_{bio} and C_{tot} strongly covary, presumably in response to atmospheric dilution resulting from changing PBL depth. The wintertime C_{bio} enhancements we observe are similar to those reported previously from the earliest part of the NHA data [*Turnbull et al.*, 2006], those inferred by Potosnak *et al.* [1999] from analysis of trace gases at nearby Harvard Forest, MA, and also from highly polluted regions in Europe [Levin *et al.*, 1980]. In the present study the contribution of C_{bio} to C_{tot} results in wintertime emissions ratios that are about a factor of two smaller than for those with respect to C_{ff}, as can be seen by comparing the range of abscissa values for wintertime results in Figs. 6b and a, respectively.

Some past studies [e.g., *Nicks et al.*, 2003] have assumed that C_{tot} and C_{ff} are equivalent. While this may be reasonable in the analysis of signals clearly in or out of a power plant plume, the wintertime contribution of C_{bio} in the US northeast suggests that C_{ff} signals would have to be ~30 ppm to avoid biases larger than ~10% resulting from the contribution of the terrestrial biosphere to total CO_2. Such high signals might be observed directly within the outflow of large point sources, but when sampling regional-scale urban/suburban signals as we do in this study, or as one might using observations from space, the total CO_2 enhancement will be much smaller. Turnbull *et al.* [2011b] observed similarly large contributions of C_{bio} to C_{tot} in a late winter/early spring aircraft sampling campaign over Sacramento, CA, where C_{ff} ranged from 0 - 10 ppm. Analysis of ^{14}C and CO_2 data from East Asia also yield a similar finding [*Turnbull et al.*, 2011a].

The large wintertime contributions of C_{bio} we observe are consistent with field observations showing substantial amounts of wintertime respiration even for colder boreal and alpine regions [e.g., *Falge et al.*, 2002; *Monson et al.*, 2006; *Wang et al.*, 2010]. Our own analysis of the surface to 4 km asl differences of C_{bio}, C_{ff} and C_{tot} in the CarbonTracker data assimilation system [*Peters et al.*, 2007, for model output see carbontracker.noaa.gov] shows that for the grid cells above CMA, C_{bio} and C_{ff} contribute about equally to the total lower troposphere enhancement in winter, consistent with our observations. Large contributions of C_{bio} to C_{tot} in winter may thus be expected, but this alone does not account for the high correlation between Δ_{gas} and C_{tot} in winter, which is in marked contrast to the highly variable C_{tot} and Δ_{gas}:C_{tot} signals seen in summer (Fig. 6a). Part of the explanation is that the winter C_{bio} signal is nearly always positive and thus of the same sign as C_{ff}, whereas the summer C_{bio} signal typically opposes C_{ff}. Additionally, we expect fluxes from respiration, which dominate in winter, to be relatively constant over days and weeks, whereas photosynthetic uptake can vary dramatically from day to day in response to weather [e.g., *Goulden et al.*, 1996], thus contributing to a noisier summertime C_{tot} distribution. The combination of relatively consistent respiratory fluxes that have accumulated in the typically stable and shallow PBL together with fossil fuel fluxes may lead to strong wintertime correlations of various anthropogenic trace gases and total CO_2. Whatever the reasons, our data demonstrate that correlations of Δ_{gas} and C_{tot} in winter are typically biased high by about a factor of two, despite the strength of the correlations.

4.2. Apparent emission ratios

Because the distributions of R_{gas} are typically both broad and non-Gaussian, we choose to characterize seasonal and year-round emission ratios using the medians of the distributions, the uncertainty of the medians, and the variability in the distributions for each gas, as listed in Table 1. An advantage of using medians in the context of our regional scale analysis is the fact that they will be less sensitive than either arithmetic means or regression slopes to ratio outliers resulting from signals in air masses in which the emissions of a given gas may not have mixed well with total regional fossil fuel-CO_2 emissions, including those from power plants, which may be decoupled from emissions closely associated with population density (see *Section 4.3* below). Medians will also be less sensitive to ratio outliers resulting from small and thus relatively uncertain C_{ff} values in the denominator of eq. 3. Uncertainties of the medians are expressed as 95% confidence intervals, which measure how well we can determine the median from the distribution. Confidence intervals were calculated using a bootstrap calculation in which each median was calculated 1000 times with randomly selected ratios drawn from the full set. (This was a bootstrap with "replacement" whereby some ratios in each random trial were repeated to keep the number of ratios used in the calculation constant). The variability around the medians is given as the 16th and 84th percentiles of the distribution.

Many time series of R_{gas} in Figure 7 show some evidence of seasonality. In order to test for seasonality of emissions more rigorously we evaluate whether the seasonal medians as determined from distributions are distinct at either the 68% or 95% confidence intervals. Of the 22 gases evaluated, 17 satisfied these criteria for seasonality (Table 1). We note that the seasonality in apparent emissions ratios we observe predominantly reflects seasonality in the emissions (or consumption by OH in the case of NMHCs) of the correlated tracer and not seasonality in the emissions of fossil fuel derived CO_2. For the US, where the national annual total during our investigation period has been about 1.6 PgC yr^{-1} (1 Pg = 10^{15}g) [*Boden et al.*, 2010], the summertime national fossil fuel CO_2 emissions are lower than wintertime ones by only ~10% [*Blasing et al.*, 2005]. For the northern US (40-50˚N), the CO_2 fossil fuel emission seasonal amplitude is slightly larger, but not likely more than 15% [*Gregg et al.*, 2009]. We also note that the seasonality of apparent emissions ratios is not an artifact of the seasonality of the C_{ff} correction, C_{corr}. Our results indicate larger emissions ratios in summer for many non-NMHC gases, whereas the impact of C_{corr} (which always increases C_{ff} and is generally greater in summer; Figure 2) would act to reduce the ratio Δ_{gas}:C_{ff} in summer relative to winter.

Below we discuss the emissions ratios and seasonality of emissions for each of the studied gases according to their primary use, source, chemistry, or regulatory control. In the case of some chemically reactive gases, we attempt to correct apparent emissions ratios for loss due to chemical destruction in summer and, for the NMHCs, to estimate time since emission based on observed summer:winter differences in apparent emissions ratio. For these calculations, we refer to estimates of atmospheric lifetimes provided in Table 2.

4.2.1 CO

For CO in summer, we obtain a median and 84th and 16th percentiles of the summertime distribution of 12 (+12/-10) ppb:ppm. The respective winter values are 11 (+9/-7) ppb:ppm. Although the winter- and summer- time distributions are similar, the time series in Figure 7 clearly shows that there are more instances of both high and low ratios during summer. As hypothesized by Turnbull *et al.* [2006], high apparent emissions ratios in summer are likely due to the presence of numerous non-fossil-fuel CO budget terms in the summer that are largely absent in the winter. Analysis of North American atmospheric CO and HCHO data by Miller *et al.* [2008] and of CO, CO_2 and C_2H_2 at Harvard Forest, MA [*Potosnak et al.*, 1999] both indicate that hydrocarbon oxidation represents a large source of CO over the US in summer.

Despite the likely presence of additional sources in summer, the raw summer- and winter- time emissions ratios as defined by medians are not distinct at their 68% confidence limits (Table 1). The lack of statistically significant seasonality in the emission ratios may be due in part to oxidation of CO by OH, which will reduce the apparent ratio in summer, but hardly at all in winter. We estimate the average July lifetime of CO as 22 days between 1000 and 600 mbar (Table 2). Assuming average travel times of ~3 days since emission as estimated independently by two different methods (*Section 4.4*), we estimate a corresponding chemical loss of 13%. Adjusting the summertime CO distributions accordingly, we obtain a median summertime emissions ratio for CO of 14 ppb/ppm and a distribution that likely better approximates the actual emissions from all sources. With this adjustment, the summer- and wintertime distributions are distinct at their 68% confidence limits (Table 2). However, much of the difference between summer and winter R_{gas} values may result from the fossil fuel emissions seasonality of 15%.

To examine instances of negative ratios of CO and other species more carefully, we use CO as a test case. Of 327 low- or mid- altitude and 4 km asl CO sample pairs, there are 20 negative $\Delta CO:C_{ff}$ ratios with relative uncertainties less than 100%. Of those, just three are clearly associated with plumes that might have resulted from long-range transport of emissions from biomass burning or upwind injection of polluted PBL air into the free troposphere. The remaining 17 could result from two situations: a) vertical wind shear in which low and high altitude samples originate from different latitudes where CO mole fractions differ; or b) enhanced chemical destruction of lower altitude samples. Both a) and b) are more likely to occur during summer and, in fact, we observe four times as many negative ratios in summer than in winter. Although more investigation is required to better understand the origin of negative ratios, they comprise only a small fraction of our samples and do not compromise our overall interpretation.

4.2.2 Halogenated Compounds

4.2.2.1 SF_6

Apparent emissions ratios of SF_6 are larger in summer than in winter at the 68% confidence interval. The dominant use of SF_6 is as a gaseous dielectric, especially in electricity transmission. Emissions are thought to be sporadic as a result of leakage

[*Olivier et al.*, 2005] and our finding of statistically significant seasonal differences is unexpected. Fossil fuel seasonality of ~15% may account for some of the observed SF_6 seasonality, but the summer and winter median values of R_{gas} differ by about ~30%. We further investigate SF_6 emissions seasonality by analyzing the vertical gradient of SF_6 at CMA for all 154 vertical profiles between 2005 and 2010. We find that summertime and wintertime differences between 0-1 km asl and 3-8 km asl observations are 0.21 ± 0.22 ppt and 0.24 ± 0.21 ppt, respectively. Despite the substantial one-sigma variability in observed gradients, the differences between the mean values and zero are statistically significant (n=50, $p \ll 0.01$). The vertical differences for the two seasons are the same within uncertainties (p=0.5). However, we expect trapping within the PBL to be greater in winter, so this suggests that summertime emissions may, in fact, be larger than in winter.

4.2.2.2 CFC Replacement compounds

With the exception of HFC-152a, all CFC replacement compounds we examined exhibit significantly higher summertime than wintertime apparent emissions ratios at their 68% confidence intervals, and HFC-134a does so at the 95% confidence interval (Table 2). Because these gases are relatively long-lived (Table 2), the apparent emission ratios primarily reflect seasonality in emissions and not chemical consumption by OH.

HFC-134a is used predominantly as a refrigerant for automobile air conditioners. The observed seasonality in R_{gas} for HFC-134a suggests that these emissions may derive largely from greater leakage from working compressors in summer; Papasavva *et al.* [2009] also suggest increased summer emissions from permeation and maintenance.

HCFC-22 is used as a refrigerant in commercial and residential air conditioners and also shows higher summertime emissions with respect to C_{ff}. Although the winter and summer R_{gas} ratios for HCFC-22 do not differ at the 95% confidence interval, it is clear from Fig. 7 that there are many instances of high summertime emissions which are not present during the winter; at the 84th percentiles (~ +1 sigma) of the respective winter and summer distributions, the winter:summer ratio is 1:2.5.

HCFC-142b is used primarily as a foam-blowing agent and also exhibits seasonality. The seasonality may be related to installation of building insulation, which is more common during summer, as is typical of most construction activities. We note, however, that the highest summer ratios are not as elevated with respect to winter as are summer ratios for either HCFC-22 or HFC-134a. HFC-143a and HFC-125 are also used as refrigerants (among other uses) and also exhibit seasonally varying emissions. In contrast, HFC-152a is used primarily as an aerosol propellant and its apparent emission ratio does not exhibit seasonality.

4.2.2.3 Dichloromethane and perchloroethylene

Dichloromethane and perchloroethylene (PCE) are solvents used primarily in populated areas with emissions therefore generally co-located with those of fossil fuel CO_2. PCE is used as a solvent in dry cleaning and industrial applications, and dichloromethane is an industrial solvent commonly used in manufacturing applications. We observe no statistically significant seasonal emission differences for either compound, even after ~6% summertime corrections for consumption by OH during summer.

4.2.2.4 Compounds controlled by the Montreal Protocol

We also examined C_{ff} correlations and R_{gas} values for CCl_4, CFC-11, CFC-12 and methyl chloroform (CH_3CCl_3), all of which are controlled under the Montreal Protocol and some of which have large Global Warming Potentials (up to 10,000 on a 100 year time horizon). Vertical contrasts between the lower troposhere and free troposphere tend to be small (Figure 5), suggesting small US emissions. Not surprisingly, correlations with C_{ff} also tend to be weak or absent. Statistically significant correlations with C_{ff} are observed only for methyl chloroform, for CFC-12 in winter, and for CFC-11 in summer. CFC-12, methyl chloroform and CCl_4 exhibit seasonality at their 68% confidence intervals, although we note that only in winter are correlations for CFC-12 statistically significant. In the cases of CFC-11, CFC-12 and methyl chloroform, inspection of the time series clearly suggest some continued emissions as evidenced by statistically significant lower troposphere enhancements.

4.2.3 Non-methane hydrocarbons

With the exception of benzene, which has been measured throughout the period of our observations, measurements for other NMHCs are available only since 2008. Nonetheless, some of these species show strong correlations with C_{ff} and all but iso-pentane show lower apparent emissions in summer than in winter (at the 68% confidence intervals). Benzene and n-butane exhibit seasonality at the 95% confidence intervals. At least some of this seasonality results from rapid oxidation of NMHCs by OH during transit to our measurement site during summer; summertime lifetimes for these NMHCs range from about 1 to 6 days (Table 2). With the exception of iso- and n-pentane, the seasonal impact of OH is also evident in Figure 5 as summertime depletions in NMHC mole fractions.

4.2.4 CH_4 and N_2O

In the coterminous US, the budgets for CH_4 and N_2O appear to be dominated by anthropogenic emissions [e.g. *Kort et al.*, 2008]. CH_4 emissions in the coterminous US are thought to be primarily from fossil fuel combustion and waste (landfills and sewage) [*European Commission*, 2009]. Accordingly, we see statistically significant correlations between CH_4 and C_{ff} in both summer and winter. We also see evidence for seasonality in CH_4 emissions (at the 68% confidence interval), with median R_{gas} 20% higher in summer than winter. While this is consistent with the expectation that temperature-sensitive wetland emissions in temperate latitudes should be strongly seasonal, there are no significant wetland sources within the fetch of our observations. The expected fossil fuel seasonality of ~15% may also explain much or all of the observed summertime increase in emissions ratio. Unlike other hydrocarbons we measure, the lifetime of CH_4 with respect to OH is several years during summer and apparent emission ratios should thus closely reflect actual emission ratios.

Although we obtain statistically significant correlations for ΔN_2O:C_{ff}, the correlations are weak. This may reflect the dominant role of agricultural (as opposed to urban) emissions in the N_2O budget, which are separated from regions of high population density where we expect R_{gas}:C_{ff} correlations to be high. The small magnitude of N_2O emissions relative to atmospheric variability and measurement noise also likely contribute to the weak correlations.. The observed seasonality of N_2O emissions may reflect their agricultural provenance in the USA.

4.3 Unexplained correlation variance

Despite the fact that most of the computed Δ_{gas}:C_{ff} correlations are significant at $p < 10^{-4}$, the median value of the year-round correlations (r^2) for all gases (excluding those restricted under the Montreal Protocol) is 0.42 (+0.07,-0.17) (+/- the 84^{th} and 16^{th} percentiles, respectively), thus leaving about 60% of the observed year-round variance unexplained. As evident from correlations in Table 1 and Figure 6b, additional variance can be explained by separating the data into seasons. With just a few exceptions (summertime CO, benzene and CH_4), separate winter and summer correlations are higher than year-round correlations, with median r^2 across all gases averaging 0.59 (+0.17/-0.23) in winter and 0.45 (+0.09/-0.17) in summer. Despite this improvement, roughly half the variance still remains unexplained.

In order to determine if separating data from the two measurement sites would further reduce variance in our results, we repeated our emissions ratio calculations for each site separately. For summer, winter and year-round, very little additional variance in Δ_{gas}:C_{ff} correlations can be explained by considering the sites separately.

Other possible sources of unexplained variance include spatial and temporal heterogeneity of tracer emissions relative to C_{ff}, and shortcomings inherent to our 1-D analysis framework. Some of the variance must result from the uncertainty in C_{ff} (i.e., 1 ppm at one sigma) which will be significant when C_{ff} is low, but the majority of unexplained variance is associated with high C_{ff} and large trace gas enhancements

(Figure 6b) which will be relatively insensitive to C_{ff} uncertainty. Heterogeneity of emission ratios can impact our analysis in several ways. First, over the years in which our measurements have been made the observing sites may have sampled different regions preferentially. Second, superimposed on the seasonality in emission ratios for many gases there appears to be additional high frequency variability in the time series of R_{gas} (Fig. 7) which could be due to temporal variability in emissions at one location and/or spatial variability that is being differently sampled by individual air samples we collect. Analysis of footprints and back-trajectories calculated using FLEXPART shows a significant sample-to-sample diversity in the regions influencing our measurements. However, we find no correlation of sample-by-sample ratios with either: a) the location of sensitivity-weighted centroid of the footprints or b) latitude or c) longitude of back-trajectories three days prior to sampling. Examination of site-based meteorological variables such as wind speed, wind direction and model-diagnosed PBL height also revealed no correlation with observed ratios. This analysis indicates that the distribution of ratios we observe, including the seasonal patterns, are not a result of changing atmospheric transport, but are likely due to spatial and temporal variations in emissions or (for reactive gases) consumption by OH.

Variation in the apparent ratios may also arise from the spatial decoupling of fossil fuel-CO_2 emissions associated with fossil fuel-based electricity generation and that from other typically urban sources such as the transportation, commercial and residential sectors. In many cases electricity generation occurs away from the populations it serves [*Gurney et al.*, 2009]. Because power plants do not emit any of the correlate gases we measure (including CO, to any reasonable degree), the power-plant fraction of C_{ff} may not always be correlated with other gases. However, as noted earlier, the relatively large distances between our observation sites and emissions should permit the full fossil fuel-CO_2 signal to mix with the correlate tracer signals most of the time.

A closer examination of the scatter plots in Fig. 6b may also provide some insight into the source of some of the residual variance. For example, the scatter plot of HFC-134a enhancements and C_{ff} shows some summertime HFC-134a samples that have much higher apparent emission ratios than the rest of the population. The same pattern is evident for some other halogenated species we measure. These samples may represent air samples in which emissions of halocarbons mixed only with fossil fuel emissions from non-power sectors such as transport and other urban sources. In addition to the higher ratios, these samples also show large absolute lower troposphere enhancements of halocarbons. The large enhancements are consistent with larger than normal PBL trapping of emissions, which would reduce the opportunity for mixing that may be required to incorporate the full range of fossil-fuel CO_2 emissions. This possibility could be tested in the future using accurate, high resolution atmospheric transport in combination with high resolution maps of CO_2 emissions such as Vulcan [*Gurney et al., 2009*].

It is instructive to compare our results to those of Turnbull *et al.* [2011b], who observed very high correlations between C_{ff} and many anthropogenic tracers, with r^2 as high as 0.9 for some hydro- and halocarbons. Whereas Turnbull *et al.* [2011b] sampled plumes directly downwind of the city of Sacramento over a just a few days in late winter/early spring (a time of year when we also observe larger correlations), in the present study, we measure signals representative of large areas over several years.

While some of the variability we observe almost certainly results from the simplicity of our 1-D analytical framework, the absence of correlation between observed emissions ratios and the footprints, back trajectories and meteorological variables suggests instead that the emissions of many gases are not entirely coherent in space and time with all components of the fossil fuel emissions. Nonetheless, of the 18 gases studied that are not controlled by the Montreal Protocol and subsequent amendments (i.e., excluding regulated gases with very low emissions), 12 display correlations with C_{ff} of $r^2 > 0.5$ in winter, and 9 do in summer.

4.4 Estimating time and distance since emission

An important aspect of our study is its region-scale nature, in that we expect the ratios we observe to be representative of emissions over scales of $10^5 - 10^6$ km^2 (as opposed to, say, 10^2 km^2). We assess this in two ways. First, we quantify the spatial sensitivity of our measurements using the average of sample "footprints" derived from the FLEXPART model (Figure 8). This analysis shows that the average center of mass of all footprints for CMA (i.e., the sensitivity-weighted centroid of the footprint) lies about 750 km away from the sampling site. Second, we use the seasonal change in apparent emission ratios of the NMHCs to estimate the time and distance since emission. Given constant atmospheric residence times since emission, the apparent emission ratios should fall on a theoretical relationship between atmospheric lifetime and winter:summer apparent emissions ratio. This relationship, expressed as the curves in Figure 9, follows the integrated rate law for first order kinetics, $[X]/[X]_o=\exp[-t/\tau]$, where t is the time since emission and τ is the pseudo first-order lifetime with respect to OH. Neglecting the small change in fossil fuel emissions between summer and winter, and assuming no change in source emissions for a given NMHC and negligible wintertime loss, $[X]/[X]_o$ is equivalent to the ratio of apparent summer to winter emission ratios.

Winter:summer ratios for 4 of 6 gases lie within the bounds of residence times of 3-5 days, which reflect the summertime transit times. We cannot use this method to derive information on winter transit times, but expect that they would be shorter, due to higher wind speeds typical for winter. The apparent ratios for iso- and n-pentane clearly fall outside of this range, even when considering the large range of emission ratios, as represented by the error bars in Figure 9. The deviation of the pentanes may indicate a flux-weighted mean emissions distance much closer than for other NMHCs or, contrary to our assumptions, that emissions for these compounds are enhanced in the summer relative to winter. The latter possibility is supported by the analysis of Lee *et al.* [2006], whose observations of iso- and n-pentane at Harvard Forest suggest higher summertime emissions; they did not find evidence of seasonality for propane or butane. Nonetheless, the lower apparent emissions ratios we observe for the majority of NMHCs in summer require significant time and distance since emission, consistent with the ~750 km length scales of surface sensitivity indicated by analysis of FLEXPART footprints. Together, these analyses indicate that our observations are regionally representative.

4.5 Estimation of "absolute" emissions from emission ratios

One of the primary advantages of linking enhancements of various anthropogenic gases to C_{ff} is that, compared to other emission inventories, fossil fuel derived CO_2 emissions are known very accurately, even though rigorously derived uncertainties for inventory-based estimates are generally not available. The few estimates of uncertainty that do exist depict high confidence in a variety of inventories. For the US, Marland *et al.* [2008] have estimated an uncertainty in the national, annual total of ~1% based on the difference between the EDGAR inventory [*Olivier et al.*, 1999] and that produced by CDIAC [*Boden et al.*, 2010], although these inventories are not entirely independent. Process-based estimates of fossil fuel-CO_2 fluxes from the Vulcan model [*Gurney et al.*, 2009] use a very different methodology and yet still agree with the economic statistics-based estimates of Boden *et al.* [2010] to within 10% at the national/annual scale. Even at the state level, Gurney *et al.* [2009] estimate uncertainties of only 8% (one-sigma). A variety of fossil fuel CO_2 inventories are now available for the US with at least monthly and state-level resolution [*Gregg et al.*, 2009; *Gurney et al.*, 2009]. Despite the absence of rigorously derived uncertainties, these estimates are likely much more accurate than those for any other gas, because of the comprehensive records of fuel sales, production and storage that are regularly reported and analyzed.

We thus estimate emissions of various anthropogenic gases by scaling the apparent atmospheric emissions ratio, R_{gas}, by the US total annual fossil CO_2 emissions of 1.6 Pg C yr^{-1} as $F_{gas}= R_{gas} \times F_{CO2}$, where F is the surface flux. To account for seasonality in R_{gas} and F_{CO2}, we scale R_{gas_summer} and R_{gas_winter} (Table 1) separately by the May-September and November-February F_{CO2}, respectively. Annual emissions are then calculated by summing the summer and winter values, weighted by the respective winter and summer F_{CO2} contributions to the annual total. This calculation assumes that the observed emission ratios for the northeastern US are valid nationally, which is a simplification we adopt until more widespread observations become available. We do not calculate absolute emissions for the northeastern US alone, as the regional “footprint” of our observations (Figure 8) does not readily correspond with political or geographical boundaries for which up-to-date independent “bottom up” estimates are available for comparison. If our assumption that northeastern US emissions ratios are representative of national emissions is valid, then the uncertainty in the absolute emissions can be accurately characterized by propagating the 95% confidence intervals for the observed winter or summer median ratios (Table 1, Figure 10). However, because we can not yet validate this assumption, we also propagate and discuss the substantially larger uncertainties based on 16th and 84th percentiles in the observed distribution of apparent emission ratios. This broader distribution may better reflect the diversity of ratios throughout the USA, and we employ them until regionally representative apparent emission ratios with associated confidence intervals are available. We note that relative to the apparent emission ratios, the uncertainty in the fossil fuel emissions (F_{CO2}) is small.

For the hydrocarbons, where it is clear that the atmospheric ratios in summertime are not representative of the actual emissions ratios, we only use the winter ratios to estimate annual emissions. We also use only the winter emission ratio for CO, where non-fossil CO budget terms such as NMHC oxidation, biomass burning and CO loss by reaction with OH are largely absent. Below, we present and discuss emissions estimates for those gases for which “bottom up” estimates are available from the US EPA National Emissions Inventory (NEI: www.epa.gov/ttn/chief/eiinformation.html), US EPA Greenhouse Gas Inventory (www.epa.gov/climatechange/emissions/usinventoryreport.html) and EDGAR [*European Commission*, 2009]. The EDGAR estimates are available only for 2005, whereas the US

EPA estimates are often available for the time interval corresponding to our observations. A comparison of the estimates is given in Table 3 and a subset is presented Figure 10.

4.5.1 CO

The median value of our national CO emissions estimate of 41 (+32/-25) Tg yr^{-1} for the period 2004-2009 is less than half the average of EPA national CO inventories for the reporting period 2005-2008, suggesting a high bias in the EPA inventories. Other studies also suggest a high bias in EPA inventories [*Miller et al.*, 2008; *Parrish*, 2006; *Turnbull et al.*, 2011b], mainly for earlier time periods. The most recent EPA inventory estimates (NEI 2008) are, however, 15% lower than 2005 estimates and 25% lower than the NEI 1999 and 2002 estimates, which were used as benchmarks in previous studies. Despite the recent declines in the EPA estimates, which bring them closer to the atmospheric observations, large discrepancies remain. These "top-down" vs. "bottom-up" differences are present not only for the aggregate 2005-2009 emissions estimate, but also for individual years (Fig. 11). Our long-term and 2005 estimates are also 15-20 Tg CO yr^{-1} lower than that from the EDGAR CO inventory for 2005, although there is overlap at the 84^{th} percentile of the distribution.

4.5.2 Halogenated Species

Our estimate of SF_6 emissions for the US of 1.4 (+1.6/-0.7) Gg SF_6 yr^{-1} exceeds the EPA inventory at the 16^{th} percentile, but is comparable to the EDGAR inventory estimate within the propagated uncertainty (Figure 10). Our estimate is also consistent with those for the US (and Canada) produced by Rigby *et al.* [2010] by inversion of atmospheric SF_6 observations (for which EDGAR was used as a prior estimate). Our US emissions estimate is about 22% of global flux as derived from the global growth rate [*Levin et al.*, 2010].

Our median emissions estimate for HFC-134a is lower than both the EDGAR and EPA inventories, but both inventories lie within the 84^{th} percentile of our estimate. The comparison to the EPA inventory is similar for HCFC-22 (Table 3), although no EDGAR inventory is available. For HCFC-142b, the EPA inventory is lower than the 16^{th} percentile of our estimate while the EDGAR inventory is similar to our median value. For HFC-152a, there is no available EPA inventory, and the EDGAR estimate just overlaps ours at the 16^{th} percentile. Our national emissions estimates for HFC-143a and HFC-125 are very similar to those of the EPA, but are, respectively, only about one third and one half that reported in EDGAR. Our PCE and dichloromethane emissions estimates are both consistent with the EPA inventories, which are available only for 2005.

For gases which have been banned by the Montreal Protocol we estimate emissions using the same method as for other gases, despite the absence of statistically significant correlations with C_{ff} in the case of CFC-11, CFC-12 and CCl_4. Our median emission estimate for CCl_4 is consistent with the value of zero Gg yr^{-1} from the EPA. While the EPA also estimates no CFC-11 emissions, the contrast between the free troposphere and lower trophosphere time series in Figure 5 suggest some continued emissions and, despite large uncertainties, our quantitative method also shows non-zero emissions at the 16^{th} percentile of variability. Despite large uncertainties, our emissions estimate for CFC-12 is consistent with that of the EPA. For methyl chloroform, for which we obtain statistically significant but weak correlations, we estimate national emissions of 2.4(+1.5/-1.4) Gg yr^{-1}. In contrast, the EPA emissions estimates have been zero Gg yr^{-1} since 1997.

4.5.3 Non-methane hydrocarbons

Benzene is the only NMHC for which up-to-date bottom-up national emission estimates are available from the EPA NEI. The EPA estimate for benzene emissions is about two times higher than our median estimate, but lies within the 84^{th} percentile (Table 3). Benzene emissions are closely linked to those for CO, because automobile exhaust represents the largest anthropogenic source for both compounds in the US. Thus, errors in EPA mobile source emissions models may help to explain biases in the inventories for both compounds. There are indications from previous studies [*Turnbull et al.*, 2011b; *Warneke et al.*, 2007] that benzene, like CO, is overestimated in the EPA inventories. However, interpretation of the prior findings is complicated by the fact that the emissions of benzene were not calculated directly but instead as emission ratios relative to CO, for which the emissions are also uncertain. In contrast, the ^{14}C-based approach is an "absolute" estimate and thus independent of any errors in CO emissions.

4.5.4 CH_4

Our median estimate of annual US CH_4 emissions is 39 (+30/-21) Tg CH_4 yr^{-1}. Anthropogenic emissions from the EDGAR inventory for 2005 is 26 Tg CH_4 yr^{-1}, and the 2005-2009 estimate from the EPA is 32 Tg CH_4 yr^{-1}. Unlike the inventories, our CH_4 estimate is not limited to anthropogenic sources, although the emission sources not counted by the inventories, such as biomass burning and wetlands, are likely to amount to just a few Tg CH_4 yr^{-1} in the coterminous US [*Fraser et al.*, 1986]. Our estimate is also consistent with top-down CH_4 inversions, which give estimates for the US in the range of 35-45 Tg CH_4 yr^{-1} for 2001 [*Bergamaschi et al.*, 2005] and summer 2003 [*Kort et al.*, 2008].

4.5.5 "Top-down" emissions uncertainty

While the ^{14}C-based estimates of US emissions for the studied suite of anthropogenic trace gases presented above are by no means definitive, they demonstrate both the promise of the approach and the usefulness of top-down, observationally-based emissions estimates in evaluating the existing bottom-up inventories. Confidence in our estimates is limited by possible differences between observed northeast US and actual national emissions ratios and the presence of unexplained variance in relationship between observed trace gas and fossil fuel CO_2 enhancements. We note that this residual variance, which we present as uncertainty, may reflect actual diversity in the spatio-temporal emissions of these gases – something that is not currently captured in inventory estimates. An inherent advantage of top-down estimates is that, unlike many bottom-up inventories, they do not require prior knowledge of all relevant emissions processes and intensities. In addition, top-down uncertainties can be quantified, as we have attempted to demonstrate. Below we evaluate possible additional sources of uncertainty or bias in the ^{14}C-based method of emissions ratio and absolute emissions detection. In addition to qualifying the current estimates, these provide a basis for improving the ^{14}C-based detection method in the future.

4.6. Methodological uncertainties

We characterize apparent emissions ratios for individual gases based on the distribution of sample-by-sample emission ratios because the observed variances can be more faithfully represented and the associated median estimates will be less sensitive to ratio outliers than would be the case using, for example, the slope of a regression of X_{obs} - X_{bg} vs. C_{ff}. A shortcoming of this approach, however, is that the individual estimates that compromise the distributions may be subject to biases in the background subtractions for CO_2, $\Delta^{14}C$, and the tracer of interest (eq. 3), and also in C_{corr} (eq. 2c).

4.6.1 Background subtraction uncertainty

In our 1-D analysis framework, we assume that the overlying free tropospheric air is the background air into which fluxes are added in (or just above) the PBL (eqs. 2a-c). However, vertical wind shear, in which the free tropospheric air originates from a different latitude than the lower troposphere air, could introduce a bias into our analysis depending on the size of the north-south gradient of a given gas. Our value of X_{bg} might be too high if, for instance, the actual background originates from a more southerly latitude (with, typically, a lower mole fraction) than the local free troposphere samples used in the analysis. For example, the difference between HFC-134a measured at the background sites Mace Head (MHD; 53˚N, 10˚W) and Kumakahi (KUM; 20˚N; 155˚W) is about 3 ppt, or 0.1 ppt/degree latitude. Thus, an average error in air origin of 20˚ of latitude might lead to an X_{bg} error of 2 ppt, which would subsequently influence the apparent emissions ratio.

Incorrect background subtraction of $\Delta^{14}C$ could also bias our analysis. For $\Delta^{14}C$ we do not have a well characterized observationally-based background. It is apparent from Figure 1 that background errors of ~3 per mil, (1 ppm C_{ff}) may be possible when strong vertical shear exists. Back-trajectories calculated by FLEXPART for CMA in summer show that our high altitude samples originate further north by ~15˚ than do those for the lower troposphere (i.e. mean wind directions of 280˚ at 4 km vs. 265˚ below 2.6 km) three days prior to sampling. Sampling the TM5 $\Delta^{14}C$ output using the end points of 7 day back trajectories for both the lower and free troposphere at CMA indicates that the free troposphere trajectories intersect $\Delta^{14}C$ values higher than those from the lower troposphere by ~1.6 ‰, (~ 0.5 ppm C_{ff}). During winter, FLEXPART back trajectories show a difference between high and low trajectories of only 3˚ of latitude three days prior to sampling, implying that the wintertime free troposphere is a better proxy of background conditions. Overall, our FLEXPART/TM5 analysis suggests that future studies of PBL enhancements of $\Delta^{14}C$ and other tracers would benefit from a fuller (i.e. two- or three- dimensional) treatment of background including stronger observational constraints, especially for $\Delta^{14}C$.

4.6.2 Correction term uncertainty

C_{corr}, as written as the second term in eq. 2c, includes only biospheric disequilibrium, but other ^{14}C budget terms such as ^{14}C from cosmogenic and nuclear reactor production may also be important (eq. 1). As with background subtraction errors, incorrect specification of C_{corr} can also result in biased estimates of C_{ff} and R_{gas}. Although the majority of cosmogenic production of ^{14}C (with subsequent oxidation to

^{14}CO and then $^{14}CO_2$) occurs in the stratosphere [*Naegler and Levin*, 2006], it is likely that there is a persistent vertical gradient in $\Delta^{14}C$ resulting from ^{14}C production, such that free troposphere values are enriched in ^{14}C relative to the PBL even in the absence of any fossil fuel emissions. While somewhat dependent on the representation of the vertical distribution of cosmogenic production, ^{14}C model simulations using TM5 show differences between 4 km asl and < 2.6 km above CMA resulting from cosmogenic production of just 0.2 ‰ (<0.1 ppm C_{ff}) with no summer-winter difference. As argued previously by Turnbull *et al.* [2009] we conclude that the lack of a cosmogenic production term in eq. 2c does not significantly influence our results.

^{14}C originating from nuclear power reactors was not included in C_{corr} or the TM5 ^{14}C simulations presented in Figure 1. If the signal from these sources is predominantly in the PBL and not in the free-troposphere, as expected, it may bias the C_{ff} calculation [*Graven and Gruber*, 2011]. All nuclear reactors in the US are either pressurized- or boiling-water reactors, both of which have been observed to produce $^{14}CO_2$ [e.g., *Dias et al.*, 2009; *Levin et al.*, 1988], although most ^{14}C from the more common pressurized-water reactors is emitted as methane, not CO_2. The distribution of nuclear reactors in the US is highly concentrated in the eastern third of the country (http://www.nrc.gov/reactors/operating/map-power-reactors.html), which is the region to which our observations are most sensitive. However, the actual magnitude of nuclear $^{14}CO_2$ emissions is poorly constrained. Our preliminary analysis of the $^{14}CO_2$ nuclear power plant signal at NHA and CMA (using FLEXPART footprints and the Graven and Gruber [2011] emissions) suggests average PBL enhancements of 1 ‰ at NHA and 2 ‰ at CMA (~0.3-0.6 ppm $C_{ff,}$ respectively). However, the point source nature of these emissions, which we and Graven and Gruber [2011] have so far treated as area sources (of 0.5x0.5˚ and 3x2˚, respectively), may result in an overestimate of the signal. Nonetheless, the small nuclear power plant "masking" of the full fossil fuel ^{14}C depletion signal suggests that our calculated values of C_{ff} are slightly too low, and thus the apparent emissions ratios and "absolute" emissions given above may be ~10-20% too high. For comparison, the average C_{ff} signal we observe in the lower altitude samples is 2.4 ppm.

We also evaluate the sensitivity of C_{ff} to the value of C_{corr} arising from our specification of the respiratory flux of ^{14}C (Figure 2) by removing the correction term in eq. 2c altogether. The average impact is to increase apparent emission ratios by 2 - 5% in both winter and summer, while the mean of r^2 values decrease by 0.04 across all gases and seasons for $C_{corr} = 0$. To further evaluate the sensitivity of our results to the specification of C_{corr}, we alternatively apply the climatological monthly mean C_{corr} values (solid curves in Fig. 2), and find average changes in ratios of just +1%. Associated r^2 values are uniformly smaller, but only by ~0.01, indicating that the climatological and sample-specific corrections provide comparable results at the seasonal and annual scale of analysis.

5. Conclusions

We have presented six years of aircraft-based atmospheric CO_2 and $\Delta^{14}CO_2$ observations from two sites in the northeast USA, which show the distinct influence of both fossil fuel-CO_2 emissions and terrestrial biosphere CO_2 sources and sinks in the lower troposphere (primarily the PBL). Lower troposphere enhancements of fossil fuel CO_2 (C_{ff}) range from -3 to 13 ppm, averaging 1.4 ppm; enhancements of biospheric CO_2

(C_{bio}) average -3.3±5.2 ppm in summer and +3.6±2.6 ppm in winter. For samples collected at ~300 m asl, the annual average C_{ff} is 2.4±2.2 ppm and summer and winter C_{bio} are -4.1±6.3 ppm and 4.6±2.5 ppm, respectively. The fossil fuel-CO_2 enhancements correlate with enhancements of a wide variety of anthropogenic trace gases throughout the year. This is in marked contrast to correlations with total CO_2, for which summer correlations are either weak or absent and for which winter correlations are biased, due to the large presence of biospheric CO_2 in the PBL, even in winter. This observation implies that any attempt to attribute CO_2 variations to anthropogenic sources using CO_2-only approaches, whether from the surface, air or space, should use additional sources of information to separately quantify the biological and fossil contributions.

Observed ratios of anthropogenic trace gas enhancements and fossil fuel CO_2 quantitatively link these enhancements to the relatively well-known emissions of fossil fuel CO_2, permitting us to calculate "absolute" emissions of the correlate gases. Future emission ratio calculations could be improved by making corrections for the small gradients in $\Delta^{14}C$ arising from nuclear production and, most importantly, by more accurately defining the background both for trace gases of interest and $\Delta^{14}C$. This will involve a better representation of the actual transport in our analysis framework and a significantly broader set of $\Delta^{14}C$ observations than exists now. Over the past 2 years, we have begun regular measurements of ^{14}C and the same large suite of anthropogenic gases at a number of upwind tower sites (see www.esrl.noaa.gov/gmd/ccgg/towers/).

The annual national fluxes for most gases we derive correspond, within uncertainties, to both EPA and EDGAR bottom-up inventories. However, our top-down calculated emissions for CO, SF_6, HCFC-142b, HFC-125, CH_2Cl_2, CH_3CCl_3 and pentanes differ from at least one of the inventories at approximately one-sigma (i.e., between the 16th and 84th percentiles in our estimates; Table 3). Currently, the emission uncertainties we estimate are large due to our use of the spread of the ratios we observe in the northeast USA as a proxy for possible national variability. However, the 95% confidence intervals for the observed emission ratios and the absolute emissions are generally much smaller and suggest that with increased spatial coverage of $\Delta^{14}C$ observations, national and regional top-down emissions estimates of many correlate gases could be determined to within 15-25% (95% confidence interval, ~ two sigma; Figure 10). Presently, the bottom-up inventories do not provide quantitative estimates of uncertainty for comparison to ours. Also, unlike inventories, our methods have the potential to provide near real-time estimates of emissions.

Finally, our results indicate that applying anthropogenic tracers as simple proxies for C_{ff} at regional scales will probably require a more detailed understanding of the budgets of these gases than currently exists. In the meantime, because none of the anthropogenic tracers we measure show strong correlations with C_{ff} throughout the year, measurements of ^{14}C will still be required to help determine fossil fuel emissions at regional scales.

Acknowledgements

SJL and JBM contributed equally to this work. We first thank the airplane pilots who made the collection of the air samples analyzed in this work possible. Numerous people contributed to the technical and logistical expertise required to operate an aircraft air-sampling program, including Doug Guenther, Sonja Wolter, Don Neff, Molly Heller, and Jack Higgs. We also thank Kelly Sours, Patricia Lang, Lloyd Miller, Carolina Siso, Steven Morgan, and Patrick Cappa for analyzing the samples; Duane Kitzis, Paul Novelli, and Brad Hall for calibrating and preparing reference gas cylinders; and Ken Masarie and Dan Chao for maintaining measurements in an easily accessible relational database. Finally, we thank Ingeborg Levin and Felix Vogel for thoughtful and detailed reviews.

References

Atkinson, R. (1997), Gas-phase tropospheric chemistry of volatile organic compounds .1. Alkanes and alkenes, *Journal of Physical and Chemical Reference Data*, *26*(2), 215-290.

Baker, A. K., A. J. Beyersdorf, L. A. Doezema, A. Katzenstein, S. Meinardi, I. J. Simpson, D. R. Blake, and F. Sherwood Rowland (2008), Measurements of nonmethane hydrocarbons in 28 United States cities, *Atmos. Environ.*, *42*(1), 170-182.

Bakwin, P. S., K. J. Davis, C. Yi, S. C. Wofsy, J. W. Munger, L. Haszpra, and Z. Barcza (2004), Regional carbon dioxide fluxes from mixing ratio data, *Tellus, Ser. B*, *56*(4), 301-311.

Bergamaschi, P., M. Krol, F. Dentener, A. Vermeulen, F. Meinhardt, R. Graul, M. Ramonet, W. Peters, and E. J. Dlugokencky (2005), Inverse modelling of national and European CH4 emissions using the atmospheric zoom model TM5, *Atmos. Chem. Phys.*, *5*(9), 2431-2460.

Blasing, T. J., C. T. Broniak, and G. Marland (2005), The annual cycle of fossil-fuel carbon dioxide emissions in the United States, *Tellus, Ser. B*, *57*(2), 107-115.

Boden, T. A., G. Marland, and R. J. Andres (2010), Global, Regional, and National Fossil-Fuel CO2 Emissions, edited, Carbon Dioxide Information Analysis Center, Oak Ridge National Laboratory, U.S. Department of Energy, Oak Ridge, Tenn., U.S.A.

Canadell, J. G., C. Le Quere, M. R. Raupach, C. B. Field, E. T. Buitenhuis, P. Ciais, T. J. Conway, N. P. Gillett, R. A. Houghton, and G. Marland (2007), Contributions to accelerating atmospheric CO2 growth from economic activity, carbon intensity, and efficiency of natural sinks, *Proceedings of the National Academy of Sciences*, *104*(47), 18866-18870.

Ciais, P., P. Friedlingstein, D. S. Schimel, and P. P. Tans (1999), A global calculation of the delta C-13 of soil respired carbon: Implications for the biospheric uptake of anthropogenic CO2, *Global Biogeochem. Cycles*, *13*(2), 519-530.

Committee on Methods for Estimating Greenhouse Gas Emissions (2010), *Verifying Greenhouse Gas Emissions: Methods to Support International Climate Agreements*, 109 pp., The National Academies Press, Washington, DC.

Dias, C. M., K. Stenstrom, I. L. Bacelar Leao, R. V. Santos, I. G. Nicoli, G. Skog, P. Ekstrom, and R. da Silveira Correa (2009), $^{14}CO_2$ dispersion around two PWR nuclear power plants in Brazil, *Journal of Environmental Radioactivity*, *100*(7), 574-580.

Dlugokencky, E. J., et al. (2009), Observational constraints on recent increases in the atmospheric CH_4 burden, *Geophys. Res. Lett.*, *36*.

European Commission, J. R. C. (2009), Emission Database for Global Atmospheric Research (EDGAR), edited.

Falge, E., et al. (2002), Seasonality of ecosystem respiration and gross primary production as derived from FLUXNET measurements, *Agricultural and Forest Meteorology*, *113*(1-4), 53-74.

Fraser, P. J., R. A. Rasmussen, J. W. Creffield, J. R. French, and M. A. K. Khalil (1986), Termites and Global Methane - Another Assessment, *J. Atmos. Chem.*, *4*(3), 295-310.

Goulden, M. L., J. W. Munger, S.-M. Fan, B. C. Daube, and S. C. Wofsy (1996), Exchange of Carbon Dioxide by a Deciduous Forest: Response to Interannual Climate Variability, *Science*, *271*(5255), 1576-1578.

Graven, H. D., and N. Gruber (2011), Continental-scale enrichment of atmospheric 14CO2 from the nuclear power industry: potential impact on the estimation of fossil fuel-derived CO2, *Atmos. Chem. Phys. Discuss.*, *11*(5), 14583-14605.

Gregg, J. S., L. M. Losey, R. J. Andres, T. J. Blasing, and G. Marland (2009), The Temporal and Spatial Distribution of Carbon Dioxide Emissions from Fossil-Fuel Use in North America, *Journal of Applied Meteorology and Climatology*, *48*(12), 2528-2542.

Gurney, K. R., D. L. Mendoza, Y. Zhou, M. L. Fischer, C. C. Miller, S. Geethakumar, and S. de la Rue du Can (2009), High Resolution Fossil Fuel Combustion CO2 Emission Fluxes for the United States, *Environmental Science & Technology*, *43*(14), 5535-5541.

Helliker, B. R., J. A. Berry, A. K. Betts, P. S. Bakwin, K. J. Davis, A. S. Denning, J. R. Ehleringer, J. B. Miller, M. P. Butler, and D. M. Ricciuto (2004), Estimates of net

CO2 flux by application of equilibrium boundary layer concepts to CO2 and water vapor measurements from a tall tower, *J. Geophys. Res.*, *109*(D20).

JCGM (2008), International Vocabulary of Metrology – Basic and General Concepts and Associated Terms, edited by J. C. f. G. i. Metrology, Bureau Internation des Poids et Mesures.

Knorr, W. (2009), Is the airborne fraction of anthropogenic CO2 emissions increasing?, *Geophys. Res. Lett.*, *36*.

Kort, E. A., J. Eluszkiewicz, B. B. Stephens, J. B. MIller, C. Gerbig, T. Nehrkorn, B. C. Daube, J. Kaplan, S. Houweling, and S. C. Wofsy (2008), Emissions of CH4 and N2O over the United States and Canada based on a receptor-oriented modeling framework and COBRA-NA atmospheric observations, *Geophys. Res. Lett.*, *35*(L18808), doi:10.1029/2008GL034031.

Krol, M., S. Houweling, B. Bregman, M. van den Broek, A. Segers, P. van Velthoven, W. Peters, F. Dentener, and P. Bergamaschi (2005), The two-way nested global chemistry-transport zoom model TM5: algorithm and applications, *Atmospheric Chemistry and Physics*, *5*, 417-432.

Lee, B. H., J. W. Munger, S. C. Wofsy, and A. H. Goldstein (2006), Anthropogenic emissions of nonmethane hydrocarbons in the northeastern United States: Measured seasonal variations from 1992–1996 and 1999–2001, *J. Geophys. Res.*, *111*(D20), D20307.

Levin, I., and U. T. E. Karstens (2007), Inferring high-resolution fossil fuel CO2 records at continental sites from combined 14CO2 and CO observations, *Tellus B*, *59*(2), 245-250.

Levin, I., B. Kromer, M. Barabas, and K. O. Munnich (1988), Environmental Distribution and Long-Term Dispersion of Reactor (Co2)-C-14 around 2 German Nuclear-Power Plants, *Health Physics*, *54*(2), 149-156.

Levin, I., B. Kromer, M. Schmidt, and H. Sartorius (2003), A novel approach for independent budgeting of fossil fuel CO2 over Europe by 14CO2 observations, *Geophys. Res. Lett.*, *30*(23), 2194.

Levin, I., K. O. Munnich, and W. Weiss (1980), The Effect Of Anthropogenic Co2 And C-14 Sources On The Distribution Of C-14 In The Atmosphere, *Radiocarbon*, *22*(2), 379-391.

Levin, I., et al. (2010), The global SF6 source inferred from long-term high precision atmospheric measurements and its comparison with emission inventories, *Atmos. Chem. Phys.*, *10*(6), 2655-2662.

Lloyd, J., et al. (2001), Vertical profiles, boundary layer budgets, and regional flux estimates for CO2 and its 13C/12C ratio and for water vapor above a forest/bog mosaic in central Siberia, *Global Biogeochem. Cycles*, *15*(2), 267-284.

Lloyd, J., et al. (2007), An airborne regional carbon balance for Central Amazonia, *Biogeosciences*, *4*(5), 759-768.

Marland, G. (2008), Uncertainties in Accounting for CO2 From Fossil Fuels, *Journal of Industrial Ecology*, *12*(2), 136-139.

Monson, R. K., D. L. Lipson, S. P. Burns, A. A. Turnipseed, A. C. Delany, M. W. Williams, and S. K. Schmidt (2006), Winter forest soil respiration controlled by climate and microbial community composition, *Nature*, *439*(7077), 711-714.

Montzka, S. A., R. C. Myers, J. H. Butler, J. W. Elkins, and S. O. Cummings (1993), Global Tropospheric Distribution and Calibration Scale of Hcfc-22, *Geophys. Res. Lett.*, *20*(8), 703-706.

Montzka, S. A., et al. (2011), Ozone-Depleting Substances (ODSs) and Related Chemicals, in *Scientific Assessment of Ozone Depletion: 2010*, edited, p. 516, World Meteorological Organization, Geneva.

Naegler, T., and I. Levin (2006), Closing the global radiocarbon budget 1945 - 2005, *J. Geophys. Res.*, *111*(D12), D12311.

Nicks, D. K., et al. (2003), Fossil-fueled power plants as a source of atmospheric carbon monoxide, *Journal of Environmental Monitoring*, *5*(1), 35-39.

Olivier, J. G. J., J. A. Van Aardenne, F. Dentener, L. Ganzeveld, and J. A. H. W. Peters (2005), Recent trends in global greenhouse gas emissions: regional trends and spatial distribution of key sources, in *Non-CO2 Greenhouse Gases (NCGG-4)*, edited by A. v. Amstel, pp. 325–330, Millpress, Rotterdam.

Olivier, J. G. J., A. F. Bouwman, J. J. M. Berdowski, C. Veldt, J. P. J. Bloos, A. H. J. Visschedijk, C. W. M. van de Maas, and P. Y. J. Zandweld (1999), Sectoral emission inventories of greenhouse gases for 1990 on per country basis as well as on 10 x 10, *Environ. Sci. Policy*, *2*, 241-264.

Papasavva, S., D. J. Luecken, R. L. Waterland, K. N. Taddonio, and S. O. Andersen (2009), Estimated 2017 Refrigerant Emissions of 2,3,3,3-tetrafluoropropene (HFC-1234yf) in the United States Resulting from Automobile Air Conditioning, *Environmental Science & Technology*, *43*(24), 9252-9259.

Parrish, D. D. (2006), Critical evaluation of US on-road vehicle emission inventories, *Atmos. Environ.*, *40*(13), 2288-2300.

Peters, W., et al. (2007), An atmospheric perspective on North American carbon dioxide exchange: CarbonTracker, *PNAS*, *104*(48), 18925-18930.

Potosnak, M. J., S. C. Wofsy, A. S. Denning, T. J. Conway, J. W. Munger, and D. H. Barnes (1999), Influence of biotic exchange and combustion sources on atmospheric CO2 concentrations in New England from observations at a forest flux tower, *J. Geophys. Res.*, *104*(D8), 9561-9569.

Randerson, J. T., I. G. Enting, E. A. G. Schuur, K. Caldeira, and I. Y. Fung (2002), Seasonal and latitudinal variability of troposphere $\Delta^{14}CO_2$: Post bomb contributions from fossil fuels, oceans, the stratosphere, and the terrestrial biosphere, *Global Biogeochem. Cycles*, *16*(4), 1112.

Rigby, M., et al. (2010), History of atmospheric SF6 from 1973 to 2008, *Atmos. Chem. Phys.*, *10*(21), 10305-10320.

Sander, S. P., et al. (2006), Chemical Kinetics and Photochemical Data for Use in Atmospheric Studies, Evaluation Number 15*Rep.*, Jet Propulsion Laboratory, Pasadena.

Spivakovsky, C. M., et al. (2000), Three-dimensional climatological distribution of tropospheric OH: Update and evaluation, *J. Geophys. Res.*, *105*(D7), 8931-8980.

Stohl, A., C. Forster, A. Frank, P. Seibert, and G. Wotawa (2005), Technical note: The Lagrangian particle dispersion model FLEXPART version 6.2, *Atmospheric Chemistry and Physics*, *5*, 2461-2474.

Stuiver, M., and H. Pollach (1977), Discussion: reporting of 14C data, *Radiocarbon*, *19*(3), 355-363.

Tans, P. P., J. A. Berry, and R. F. Keeling (1993), Oceanic $^{13}C/^{12}C$ observations: A new window on ocean CO_2 uptake, *Global Biogeochem. Cycles*, *7*(2), 353-368.

Thompson, M. V., and J. T. Randerson (1999), Impulse response functions of terrestrial carbon cycle models: method and application, *Global Change Biology*, *5*(4), 371-394.

Thoning, K. W., P. P. Tans, and W. D. Komhyr (1989), Atmospheric carbon dioxide at Mauna Loa Observatory 2. Analysis of the NOAA GMCC data, 1974-1985, *J. Geophys. Res.*, *94*, 8549-8565.

Turnbull, J., P. Rayner, J. Miller, T. Naegler, P. Ciais, and A. Cozic (2009), On the use of 14CO2 as a tracer for fossil fuel CO2: Quantifying uncertainties using an atmospheric transport model, *J. Geophys. Res.*, *114*.

Turnbull, J. C., J. B. Miller, S. J. Lehman, P. P. Tans, R. J. Sparks, and J. Southon (2006), Comparison of (CO2)-C-14, CO, and SF6 as tracers for recently added fossil fuel CO2 in the atmosphere and implications for biological CO2 exchange, *Geophys. Res. Lett.*, *33*(1).

Turnbull, J. C., S. J. Lehman, J. B. Miller, R. J. Sparks, J. R. Southon, and P. P. Tans (2007), A new high precision 14CO2 time series for North American continental air, *J. Geophys. Res.*, *112*(D11), D11310.

Turnbull, J.C., Tans, P.P, Lehman, S.J., Baker, D., Conway, T.J., Chung, Y.S., Gregg, J., Miller, J.B., Southon, J.R., and L-X. Zhou (2011a). Atmospheric observations of carbon monoxide and fossil fuel CO_2 emissions from East Asia. *J. Geophys. Res.*

116, (D24306), doi:10.1029/2011JD016691.

Turnbull, J. C., et al. (2011b), Assessment of fossil fuel carbon dioxide and other anthropogenic trace gas emissions from airborne measurements over Sacramento, California in spring 2009, *Atmospheric Chemistry and Physics*, *11*(2), 705-721.

Vogel, F. R., S. Hammer, A. Steinhof, B. Kromer, and I. Levin (2010), Implication of weekly and diurnal 14C calibration on hourly estimates of CO-based fossil fuel CO2 at a moderately polluted site in southwestern Germany, *Tellus B*, *62*(5), 512-520.

Wang, T., et al. (2010), Controls on winter ecosystem respiration at mid- and high-latitudes, *Biogeosciences Discuss.*, *7*(5), 6997-7027.

Warneke, C., et al. (2007), Determination of urban volatile organic compound emission ratios and comparison with an emissions database, *J. Geophys. Res.*, *112*(D10), D10S47.

Wilson, E. W., W. A. Hamilton, H. R. Kennington, B. Evans, N. W. Scott, and W. B. DeMore (2006), Measurement and estimation of rate constants for the reactions of hydroxyl radical with several alkanes and cycloalkanes, *Journal of Physical Chemistry A*, *110*(10), 3593-3604.

Figure Captions

Figure 1. Model representations of $\Delta^{14}C$ (left panel) and the fossil fuel component of total CO_2 (C_{ff}; right panel) in the atmosphere near the surface over North America. Simulations were performed using the TM5 model at 1˚x1˚ over North America with inputs for all CO_2 and $\Delta^{14}C$ budget terms listed in eqs. 1 a and b, with the exception of nuclear reactor emissions. The fossil fuel emissions used in the model are the same as those used in the CarbonTracker data assimilation and are based on the CDIAC USA and global totals [Boden et al., 2009], USA national seasonality [Blasing *et al.*, 2005] and the spatial patterns from the EDGAR inventory (see carbontracker.noaa.gov). The color scales in the two panels are not adjusted to maximize similarity between the $\Delta^{14}C$ and C_{ff} per se, but rather scaled to the theoretical relationship between C_{ff} and $\Delta^{14}C$ of -2.7 ‰ ppm^{-1}.

Figure 2. The correction term, C_{corr}, (see eq. 2b) for all samples by month for site CMA. Red circles are individual corrections for lower altitude samples (~ 300 m asl) and pink circles are corrections for mid-level altitudes (~2100 m asl). Solid lines with error bars show monthly averages for both altitudes.

Figure 3. Example vertical profiles above site CMA (offshore from Cape May, NJ) from Feb. 21, 2007 (a) and above site NHA (offshore from Portsmouth, NH) July 10, 2008. Black, red and green pluses connected with a line represent nine air samples collected between the surface and 8 km asl, and analyzed for CO_2, CO, and HFC-134a,

respectively. Note that many additional compounds are measured in these samples. Orange circles represent values from the three altitudes at which $\Delta^{14}C$ is analyzed. The first example shows a typical profile in which CO_2, CO and HFC-134a are elevated and $\Delta^{14}C$ is depleted, due to anthropogenic emissions. The second example shows a summertime example where fossil fuel CO_2 is masking the true extent of net photosynthetic uptake by the terrestrial biosphere.

Figure 4. Observations of CO_2 and $\Delta^{14}C$ used in this study. The top panel shows the subset of CO_2 observations from NHA and CMA for which we also have $\Delta^{14}C$ observations. Blue colors (cyan = NHA; grey-blue = CMA) represent those samples above 2600 m asl (typically ~ 4 km asl), which we take to be background samples in eqs 2a-c; black/grey colors (black = NHA; grey = CMA) represent samples below 2600 m asl. The middle panel shows the values of $\Delta^{14}C$ for the same air samples. The main lower panel shows the lower troposphere CO_2 enhancement or depletion (C_{tot}, black) split into fossil (C_{ff}, red) and terrestrial biological (C_{bio}, green) components using eqs 2a-c. The lower right-hand panel is a projection of C_{ff} and C_{bio} onto the vertical axis as a histogram.

Figure 5. Time series of the 22 anthropogenic gases to which we compare derived C_{ff}. As in Figure 4, blue represents samples collected above 2600 m asl and black represents samples below 2600 m asl.

Figure 6 a and b. Scatter plots of ΔCO_2 (lower troposphere minus free troposphere CO_2, referred to as C_{tot} in the text), (6a) or C_{ff} (6b) versus $\Delta_{gas\_}$(lower troposphere minus free troposphere differences of the anthropogenic gases listed in Table 1). Red circles represent samples collected between May and September and blue circles represent samples collected between December and February. Grey circles represent samples collected during other months. Open circles represent our "mid-level" samples from 2000 – 2600 m asl; closed circles represent lower level samples 300-600 m asl. All plots have the same x-axis (CO_2) scales and the y-axis scales are the same for individual gases in Figures 6a and 6b. X and Y error bars are plotted for all summer and winter data, although in many cases error bars are smaller than the symbol sizes. r^2 values are printed on each graph and colored according to season for all regressions in which the r^2 is significantly different from zero at $p < 0.05$ (two-tailed).

Figure 7. Time series of ratios determined for individual samples (left panels) and histograms of ratios (right panels). As with Figure 6, red represents summer ratios, blue represents winter ratios and grey, other months. In the histograms, adjacent grey, blue and red bars each share a single bin. For example, for CO, there are comparable frequencies of ratios in the 0-10 ppb/ppm bin for summer, winter, and other months as indicated by adjacent bars.

Figure 8. Average footprint for all samples collected at CMA below 2600 m asl. Footprints were calculated using the FLEXPART Lagrangian particle dispersion model as described in the text. The green crosshair is the release point (the location of the site

CMA) and the green square is the 'centroid' of the footprint, that is, the point at which footprint contributions are equal to the north and south and east and west, respectively.

Figure 9. July atmospheric lifetime for non-methane hydrocarbons plotted against the apparent winter:summer emissions ratio. Values are taken from Table 2. Also plotted in grey are theoretical relationships between winter:summer apparent emission ratios (given aseasonal emissions) for atmospheric residence times between 1 and 5 days (denoted by numerals atop the curves), based on the integrated 1st order rate equation: $[X]=[X]_0\exp[-t/\tau]$, where $[X]_0$ and $[X]$ are the winter and summer NMHC concentrations, respectively. Note that C_{ff}, the denominator of the apparent emission ratio is not impacted by reaction with OH. The error bars are calculated by propagating the 95% confidence intervals (taken as the average of the +47.5% and -47.5%) through the quotient of the winter:summer ratio.

Figure 10. Emissions of selected gases for the USA derived from annual median atmospheric ratios (blue); EPA emission estimates (red) and EDGAR emission estimates (yellow). Black error bars are the propagated 16th and 84th percentiles of the apparent emission ratio distribution, and green error bars represent the 95% confidence intervals of the median emission values. This calculation assumes that the emission ratios derived for the northeast US are valid nationally and we include the (generally) larger distribution-based error bars as a proxy for unaccounted for differences between northeastern and national apparent emission ratios (see main text).

Figure 11 CO emissions for the USA for 2006-2009 derived from wintertime median atmospheric ratios (blue); EPA emission estimates (red) and EDGAR emission estimates (yellow). Top-down, C_{ff}-based emissions are plotted on the year boundary to reflect the fact that they are calculated using November-February ratios, whereas inventory-based emissions are plotted at mid-year. 2005-2009 emissions and uncertainty from Table 3 are shown as the grey solid and dashed lines. As with Figure 10, error bars (blue and grey) are the propagated 16th and 84th percentiles of the atmospheric ratio distribution transformed into emissions. Green error bars for the C_{ff}-based emissions are the 95% confidence intervals of the medians, derived from a bootstrap (with replacement) calculation. Blue numbers across the x-axis reflect how many wintertime measurements were used in the calculations.

Table 1a. Year-round median apparent ratios (R_{gas})[1]

Gas	Median	16^{th} – 84^{th} %ile[2]	95% Conf. Int.[3]	r^2	p[4]	Unc.[5] (%)
CO	11.2	3.4 - 23.0	9.6 - 13.2	0.48	0	0.50
SF_6	0.069	0.03 - 0.17	0.060 - 0.081	0.33	0	0.50
HFC-134a	3.0	0.53 - 7.1	2.5 - 3.6	0.43	0	0.50
HCFC-22	5.0	1.3 - 11.4	4.3 - 5.8	0.46	0	0.20
HFC-125	0.8	0.28 - 1.9	0.7 - 1.0	0.44	0	0.30
HFC-152a	2.7	0.9 - 6.1	2.3 - 3.1	0.41	0	4.00
HFC-143a	0.5	0.21 - 1.0	0.4 - 0.6	0.55	0	1.00
HCFC-142b	0.4	0.13 - 1.0	0.3 - 0.6	0.57	0	1.00
C_2Cl_4	1.3	0.38 - 3.4	1.1 - 1.5	0.45	0	0.80
CH_2Cl_2	1.9	0.42 - 5.3	1.5 - 2.6	0.34	0	0.70
CFC-11	1.0	0.28 - 2.3	0.7 - 1.2	0.14	0	0.50
CFC-12	0.8	0.34 - 1.9	0.6 - 1.4	0.04	0.057	0.50
CH_3CCl_3	0.2	0.08 - 0.36	0.1 - 0.2	0.14	1.0E-5	0.50
CCl_4	0.0	-0.5 - 0.48	-0.3 - 0.3	0.00	0.8	0.50
C_6H_6	10.2	2.21 - 20.6	8.2 - 12.3	0.32	0	0.20
C_3H_8	138	56.1 - 286	113.3 - 163	0.24	1.2E-7	0.10
nC_4H_{10}	36.2	14.1 - 108.7	28.4 - 55	0.19	8.5E-6	1.70
nC_5H_{12}	14.0	5.7 - 31.4	9.6 - 19.3	0.31	0	0.17
iC_5H_{12}	29.5	9.2 - 60.4	23.2 - 37.8	0.46	0	0.50
C_2H_2	34.2	9.1 - 67.5	28.6 - 37.6	0.40	0	1.00
CH_4	17.3	8.8 - 32.8	16.0 - 19.8	0.48	0	0.05
N_2O	0.31	0.13 - 0.68	0.28 - 0.37	0.11	0	0.10

Table 1b. Summer median apparent ratios (R_{gas})[1]

Gas	Median	16^{th} – 84^{th} %ile[2]	95% Conf. Int.[3]	r^2	p[4]
CO	12.2	1.8 - 24.1	9.7 - 14.8	0.38	0
SF_6	0.082	0.04 - 0.19	0.067 - 0.113	0.34	0
HFC-134a	4.4	0.75 - 8.9	3.5 - 6.2	0.51	0
HCFC-22	6.5	1.6 - 16.6	4.9 - 8.4	0.52	0
HFC-125	1.0	0.42 - 2.1	0.8 - 1.4	0.54	0
HFC-152a	2.9	1.5 - 6.3	2.1 - 3.9	0.42	0
HFC-143a	0.5	0.34 - 1.3	0.4 - 1.0	0.61	0
HCFC-142b	0.5	0.19 - 1.0	0.4 - 0.7	0.72	0
C_2Cl_4	1.5	0.45 - 3.5	1.2 - 1.8	0.50	0
CH_2Cl_2	2.2	0.64 - 7.1	1.6 - 3.7	0.40	0
CFC-11	1.0	0.64 - 2.8	0.8 - 1.6	0.23	1.2E-07
CFC-12	1.0	0.51 - 2.8	0.6 - 1.5	0.01	0.40
CH_3CCl_3	0.2	0.09 - 0.43	0.1 - 0.3	0.05	0.088
CCl_4	-0.3	-1.1 - 0.48	-0.5 - 0.3	0.00	0.6
C_6H_6	7.3	-0.23 - 14.8	4.7 - 9.8	0.20	3.6E-07
C_3H_8	113	41.2 - 163	84.3 - 138	0.53	0
nC_4H_{10}	27.5	7.1 - 60.3	14.9 - 35	0.42	2.4E-7
nC_5H_{12}	10.7	4.9 - 24.3	8.1 - 18.7	0.38	2.4E-07
iC_5H_{12}	29.6	17.2 - 54.1	27.4 - 42.1	0.47	0
C_2H_2	26.6	8.0 - 45.1	12.9 - 34.2	0.50	0
CH_4	19.8	10.0 - 36.5	16.3 - 22.2	0.43	0
N_2O	0.37	0.12 - 0.80	0.24 - 0.56	0.10	1.7E-05

Table 1c. Winter median apparent ratios (R_{gas})[1]

Gas	Median	$16^{th} – 84^{th}$ %ile[2]	95% Conf. Int.[3]	r^2	p[4]
CO	10.9	4.3 - 19.5	8.8 - 14.3	0.60	0
SF_6	0.060	0.02 - 0.11	0.042 - 0.082	0.50	0
HFC-134a	2.1	0.78 - 3.3	1.6 - 2.8	0.77	0.
HCFC-22	4.7	1.6 - 6.6	3.3 - 5.1	0.79	0.
HFC-125	0.6	0.32 - 1.5	0.6 - 0.7	0.58	0.
HFC-152a	2.6	0.9 - 4.9	1.8 - 3.0	0.42	9.5E-07
HFC-143a	0.4	0.31 - 0.7	0.3 - 0.6	0.82	4.8E-07
HCFC-142b	0.2	0.18 - 0.6	0.2 - 0.6	0.65	9.8E-05
C_2Cl_4	1.2	0.42 - 2.1	0.9 - 1.7	0.75	0
CH_2Cl_2	1.9	0.97 - 3.5	1.4 - 2.6	0.38	5.1E-06
CFC-11	0.6	0.22 - 3.4	0.2 - 1.5	0.08	0.054
CFC-12	0.5	0.34 - 1.1	0.3 - 0.7	0.30	0.023
CH_3CCl_3	0.1	0.05 - 0.22	0.1 - 0.2	0.35	7.4E-04
CCl_4	0.0	-0.3 - 0.68	-0.3 - 0.2	0.01	0.67
C_6H_6	17.0	10.18 - 34.6	14.2 - 26.3	0.63	0
C_3H_8	265	42.7 - 922	134.4 - 301	0.29	0.025
nC_4H_{10}	102.8	16.9 - 308.2	48.9 - 123	0.36	0.011
nC_5H_{12}	29.7	5.7 - 75.7	16.7 - 34.4	0.42	4.7E-03
iC_5H_{12}	42.2	4.6 - 82.4	17.4 - 60.5	0.59	3.4E-04
C_2H_2	45.9	28.6 - 113.1	28.6 - 102.9	0.69	1.2E-04
CH_4	16.5	7.0 - 27.8	14.0 - 21.5	0.65	0
N_2O	0.21	0.12 - 0.38	0.17 - 0.31	0.18	3.0E-04

1. Units for all emission ratios are ppt:ppm, except for CO, CH_4 and N_2O which are ppb:ppm and are derived from all available data at both sites between 2004 and the end of 2009.
2. The $16^{th} – 84^{th}$ percentiles of the distribution of medians (equivalent to one sigma if the distribution were Gaussian.)
3. 95% confidence intervals ($2.5^{th} – 97.5^{th}$ %iles) for median value calculated using a bootstrap technique as described in the text.
4. p - values are two-tailed, calculated using a student's t-test; p-values of zero represent values less than 10^{-8}, the precision of the calculation.
5. Unc. is the one sigma measurement repeatability for each gas, expressed as percent.

Table 2. Emissions Ratio Seasonality and Lifetimes with respect to OH

Gas	Win/Sum AER[1]	Seasonal?[2]	Lifetime Units	Jan.[4]	July	Ref
CO	0.90	1[3]	Day	254	22	5
SF_6	0.73	1	Yr	∞	∞	N/A
HFC-134a	0.48	2	Yr	101	5	5
HCFC-22	0.72	1	Yr	90	4	5
HFC-125	0.48	1	Yr	232	11	5
HFC-152a	0.90	0	Yr	9	0.54	5
HFC-143a	0.69	1	Yr	426	19	5
HCFC-142b	0.59	1	Yr	141	7	5
C_2Cl_4	0.85	0	Day	771	42	6
CH_2Cl_2	0.87	0	Day	1061	63	5
CFC-11	0.47	0	Yr	373401	10238	5
CFC-12	0.13	1	Yr	250645	7075	5
CH_3CCl_3	0.63	1	Yr	42	2.12	5
CCl_4	-0.06	1	Yr	1461	60	5
C_6H_6	2.34	2	Day	63	4.5	6
C_3H_8	2.34	1	Day	86	5.5	6
nC_4H_{10}	3.73	2	Day	35	2.4	6
nC_5H_{12}	2.77	1	Day	21	1.4	6
iC_5H_{12}	1.42	0	Day	18	1.6	7
C_2H_2	1.73	1	Day	72	6.1	5
CH_4	0.83	1	Yr	76	3.6	5
N_2O	0.56	1	Yr	∞	∞	N/A

1. Winter:Summer apparent emission ratios derived from medians in Table 1.
2. Numbers represent whether uncertainties for winter and summer emission ratios are distinct at the 68% confidence interval (1), 95% confidence interval (2) or not at all (0). Confidence intervals are determined from a bootstrap calculation, with replacement, (n=1000) of summer and winter medians.
3. Only after correcting for estimated loss due to OH are winter and summer CO 68% confidence intervals distinct.
4. Lifetimes are determined using average OH concentrations [*Spivakovsky et al.*, 2000] from 1000 – 600 hPa in the global 36-44˚ latitude band for January and July and temperature (and some pressure) dependent rate constants [*Atkinson*, 1997; *Sander et al.*, 2006; *Wilson et al.*, 2006] in combination with the lapse rate taken from the US Standard Atmosphere.
5. Sander *et al.* 2006
6. Atkinson, 1997
7. Wilson *et al.*, 2006

Table 3. Estimates of US Emissions[1] from top-down and bottom-up approaches

	^{14}C-based		Inventory			
Gas	Median	Range[2]	EPA	EDGAR[8]	Global[9]	% Global
CO	41	16 - 73	77[3]	62		
SF_6	1.4	0.7 - 3.0	0.7[4]	1.8	6.3	22
HFC-134a	46	10 - 86	55[4]	70	140	33
HCFC-22	66	19 - 138	85[5]		355	18
HFC-125	6.2	3.0 - 13.2	5.4[4]	10	22	28
HFC-152a	25	11 - 50		12		
HFC-143a	5.2	3.6 - 11.3	4.4[4]	12	17	31
HCFC-142b	11	5.0 - 24.1	3.3[5]	12	39	29
C_2Cl_4	28	9.3 - 46.4	32[6]			
CH_2Cl_2	22	11 - 39	46[6]			
CFC-11	10	4 - 61	11[5]		77	14
CFC-12	12	7 - 32	7[5]		70	18
CH_3CCl_3	2.4	1.0 – 3.9	0[5]		8	31
CCl_4	0.4	-5.6 - 14	0[5]		59	4
C_6H_6	177	106 - 360	351[6]			
C_3H_8	1074	246 - 3008	543[7]			
nC_4H_{10}	481	90 - 1350	1753[7]			
nC_5H_{12}	187	51 - 461	1624[7]			
iC_5H_{12}	340	109 - 645				
C_2H_2	123	0.1 - 264.8	131[7]			
CH_4	39	18 - 69	32[4]	26	550	7
N_2O	1.7	0.7 - 3.6	1.0[4]	1.0	53	3

1. Units are Gg yr^{-1} for all gases except, CH_4, N_2O, and CO which are Tg yr^{-1} and are derived from separate consideration of summer and wintertime R_{gas} ratios and fossil fuel emissions (see main text).
2. Range is the 16th and 84th percentile of the calculated distribution of emissions as described in the text.
3. Average of 2005-2008; NEI Criteria Air Pollutants Trends
4. Average of 2005-2009; U.S. GHG Inventory 2011, Draft
5. Average of 2005-2009; Dave Godwin, US EPA, personal communication
6. NEI, 2005.
7. In the NEI 2005, VOCs as a class are included, but are not separated by compound. Emissions for compounds other than benzene are calculated using speciation factors provided by the EPA. In the cases of butane and pentane, no isomeric speciation information is provided, so EPA values given are for both n- and iso- isomers.
8. 2005 values from EDGAR v 4.1
9. The global percentage of US $\Delta^{14}C$-based emissions. 2000-2008 values from NOAA/ESRL globally averaged marine boundary layer growth rates for long-lived species using mean lifetimes from Table 2, except for HFC-143a, HFC-125, CFC-11, CH_3CCl_3 and CCl_4, which are taken from *Scientific Assessment of Ozone Depletion: 2010.* N_2O value from Hirsch et al, 2006.

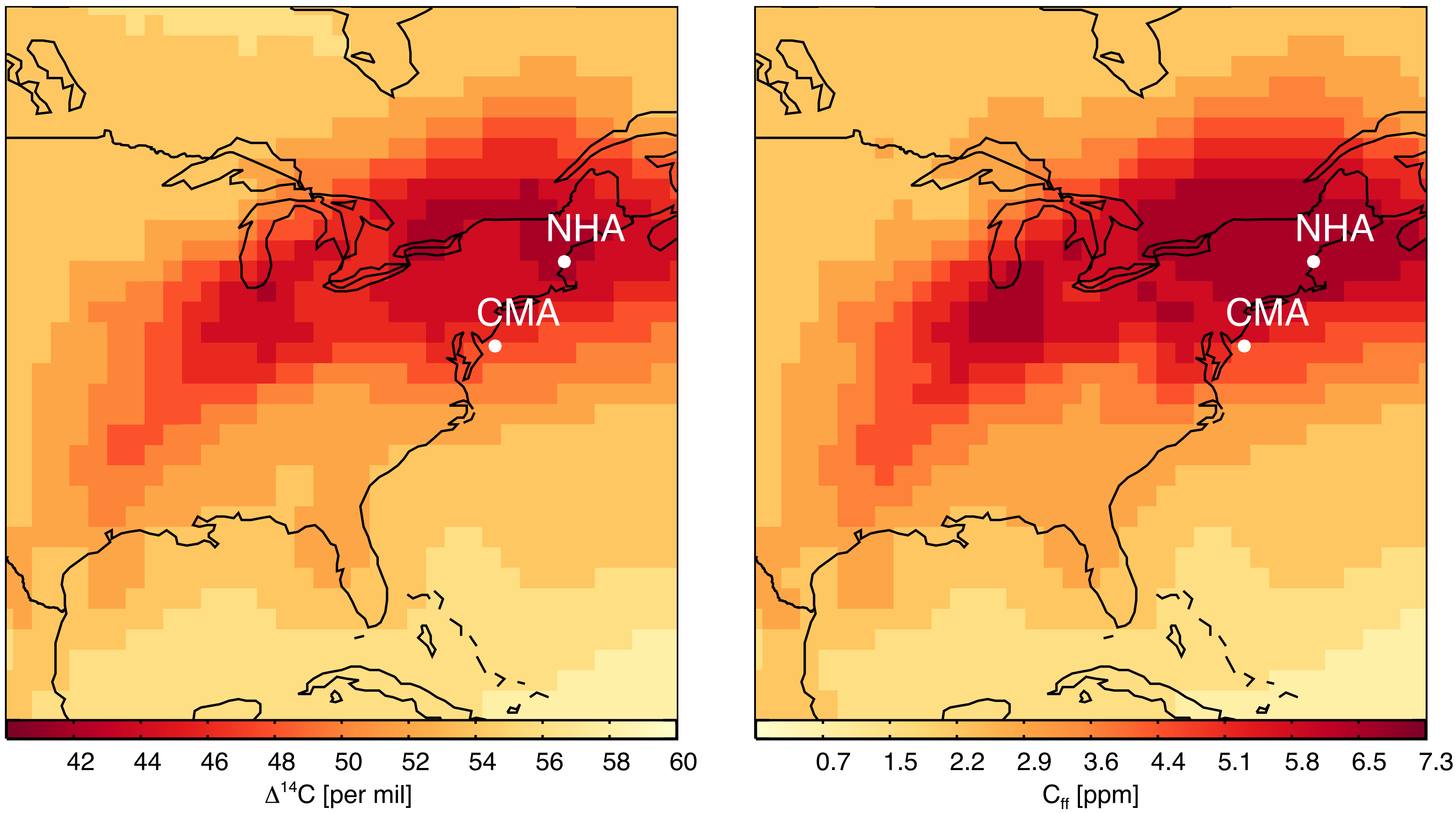
NHA
CMA
42 44 46 48 50 52 54 56 58 60
Δ14C [per mil]
NHA
CMA
0.7 1.5 2.2 2.9 3.6 4.4 5.1 5.8 6.5 7.3
Cff [ppm]

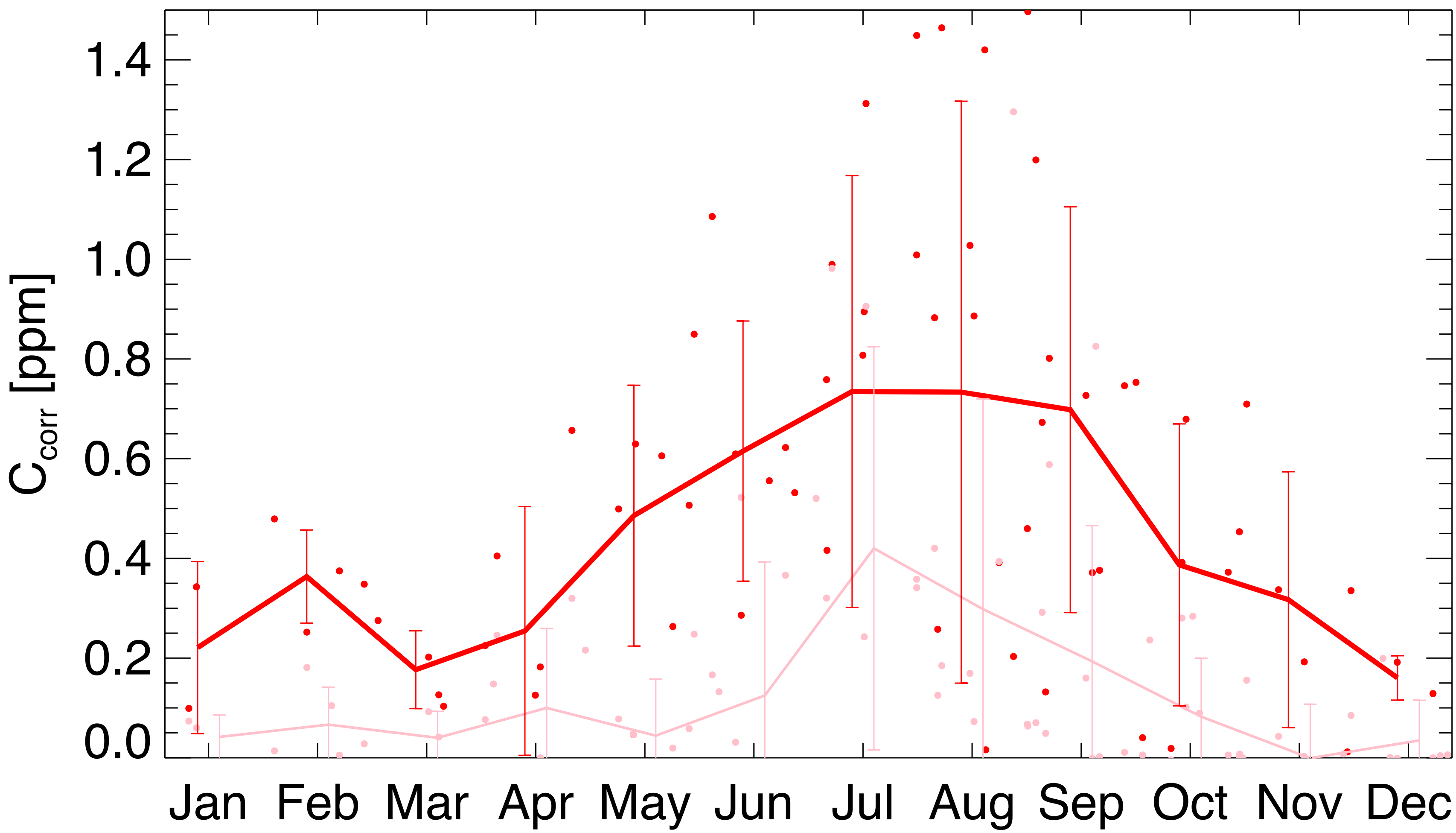

C_{corr} [ppm]
0.0
0.2
0.4
0.6
0.8
1.0
1.2
1.4
Jan
Feb
Mar
Apr
May
Jun
Jul
Aug
Sep
Oct
Nov
Dec

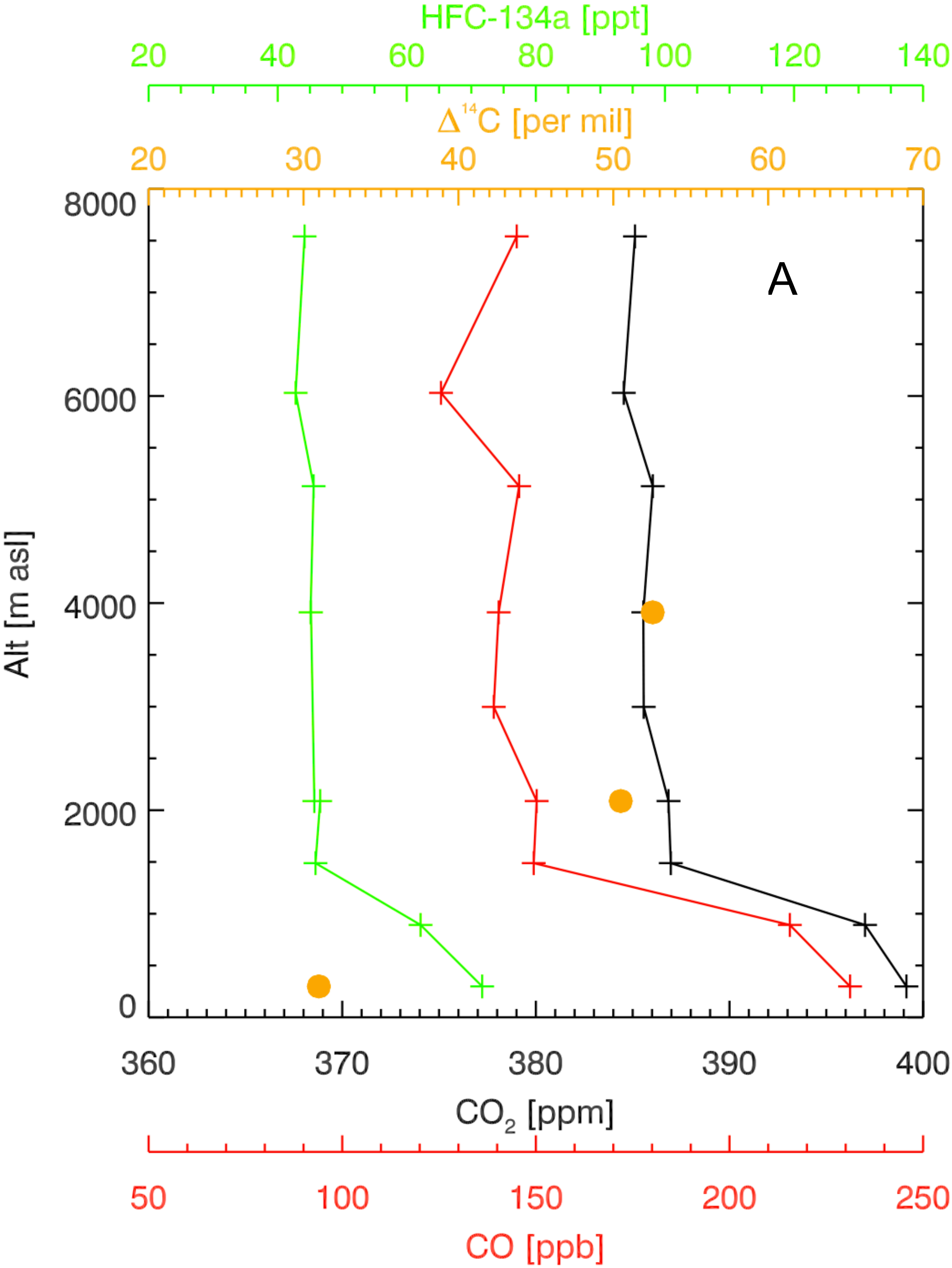
HFC-134a [ppt]
20 40 60 80 100 120 140
Δ14C [per mil]
20 30 40 50 60 70
A
Alt [m asl]
8000 6000 4000 2000 0
360 370 380 390 400
CO2 [ppm]
50 100 150 200 250
CO [ppb]

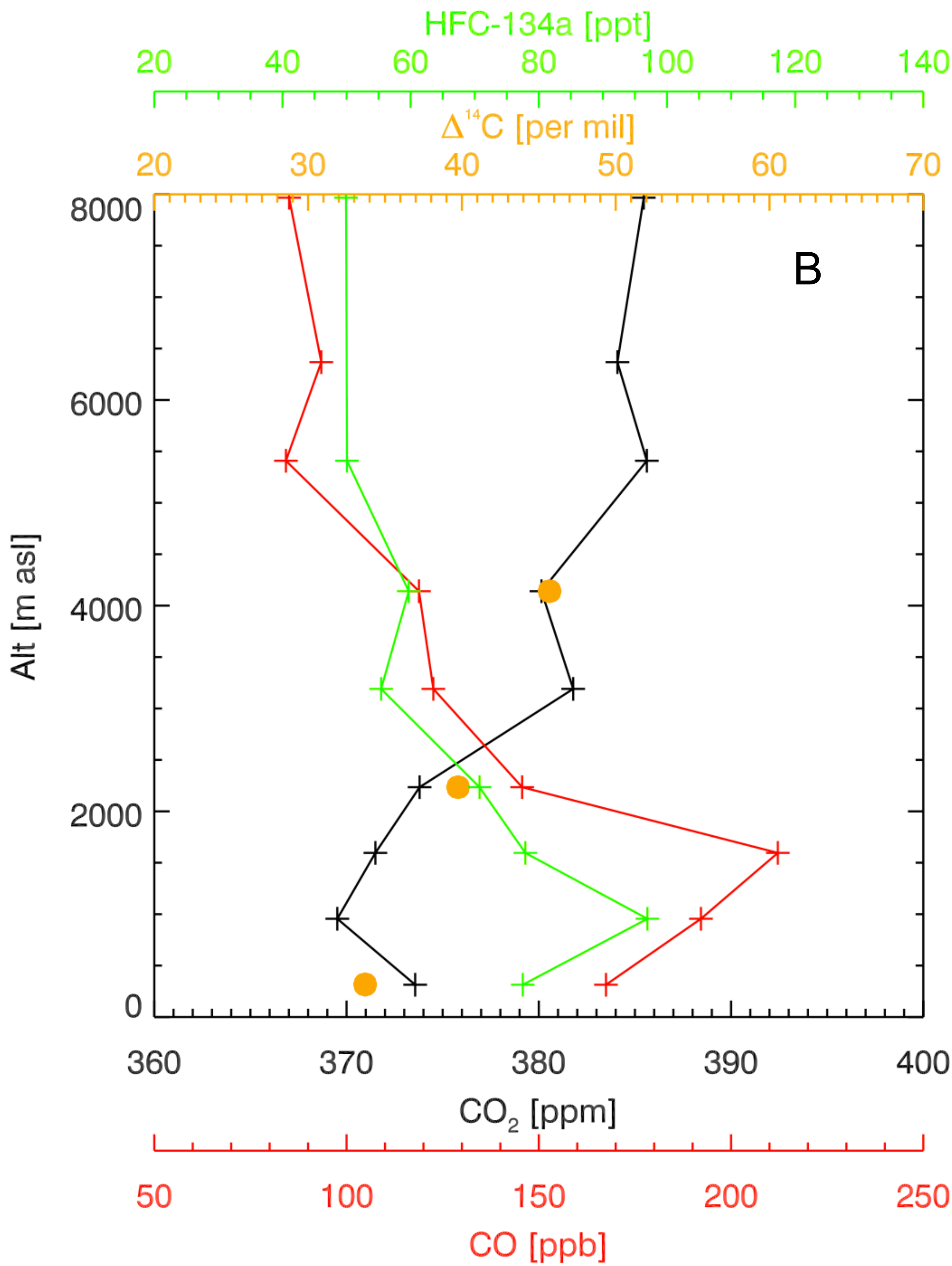
HFC-134a [ppt]
20
40
60
80
100
120
140
Δ14C [per mil]
20
30
40
50
60
70
B
8000
6000
4000
2000
0
Alt [m asl]
360
370
380
390
400
CO2 [ppm]
50
100
150
200
250
CO [ppb]

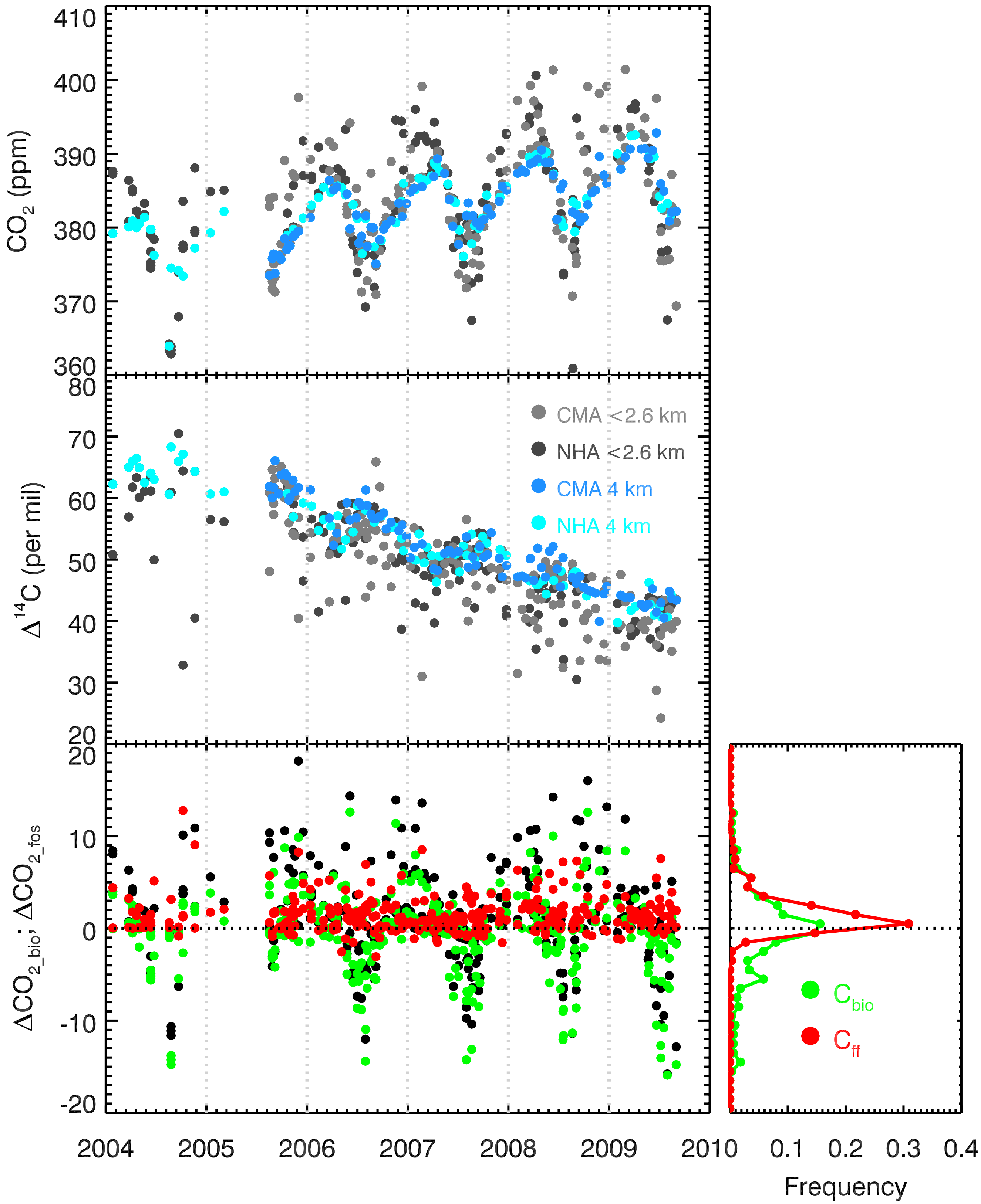

CO2 (ppm)
Δ14C (per mil)
ΔCO2_bio; ΔCO2_fos
CMA <2.6 km
NHA <2.6 km
CMA 4 km
NHA 4 km
Cbio
Cff
Frequency
2004
2005
2006
2007
2008
2009
2010

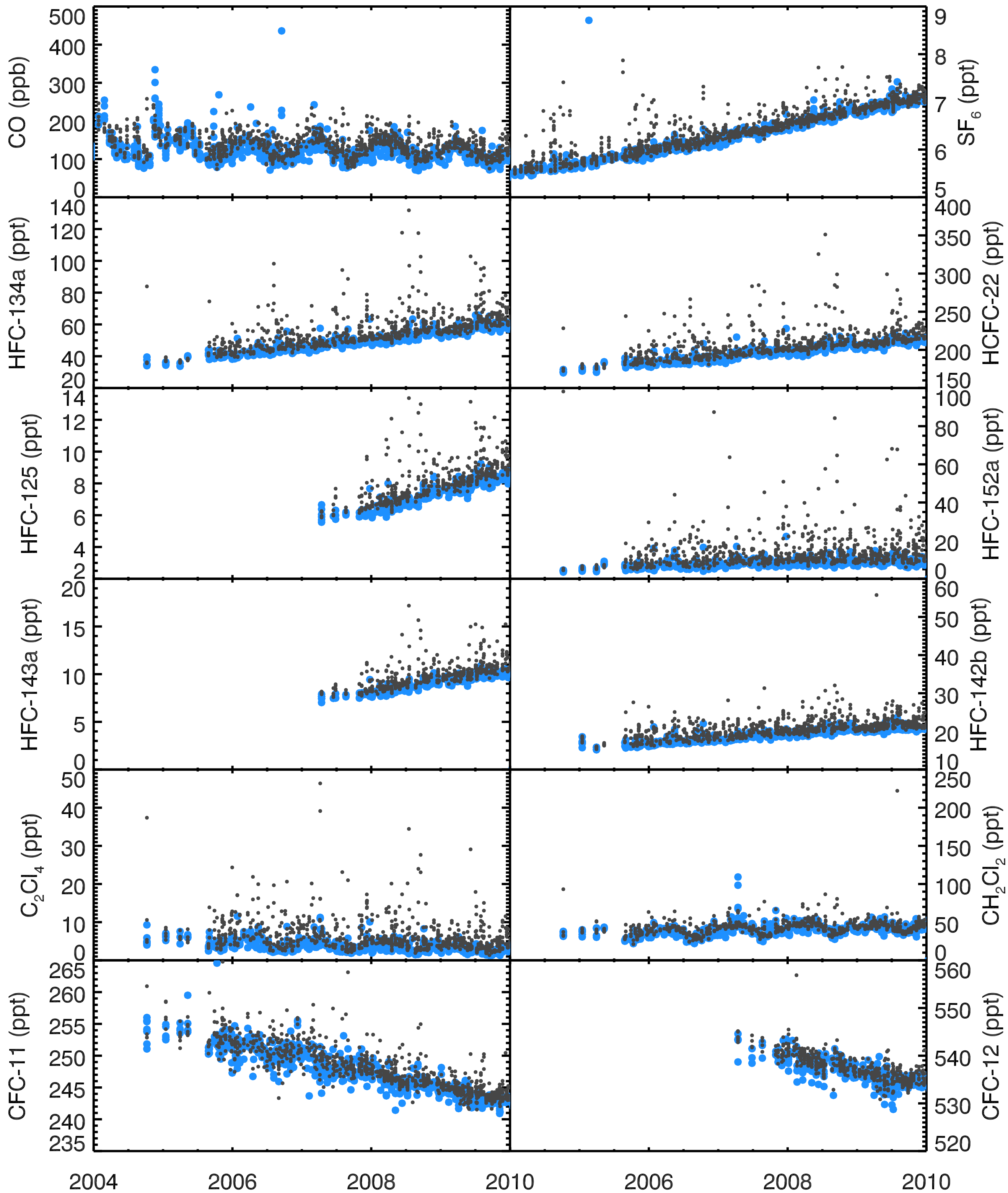

CO (ppb)
SF$_6$ (ppt)
HFC-134a (ppt)
HCFC-22 (ppt)
HFC-125 (ppt)
HFC-152a (ppt)
HFC-143a (ppt)
HFC-142b (ppt)
C$_2$Cl$_4$ (ppt)
CH$_2$Cl$_2$ (ppt)
CFC-11 (ppt)
CFC-12 (ppt)
2004
2006
2008
2010
2006
2008
2010

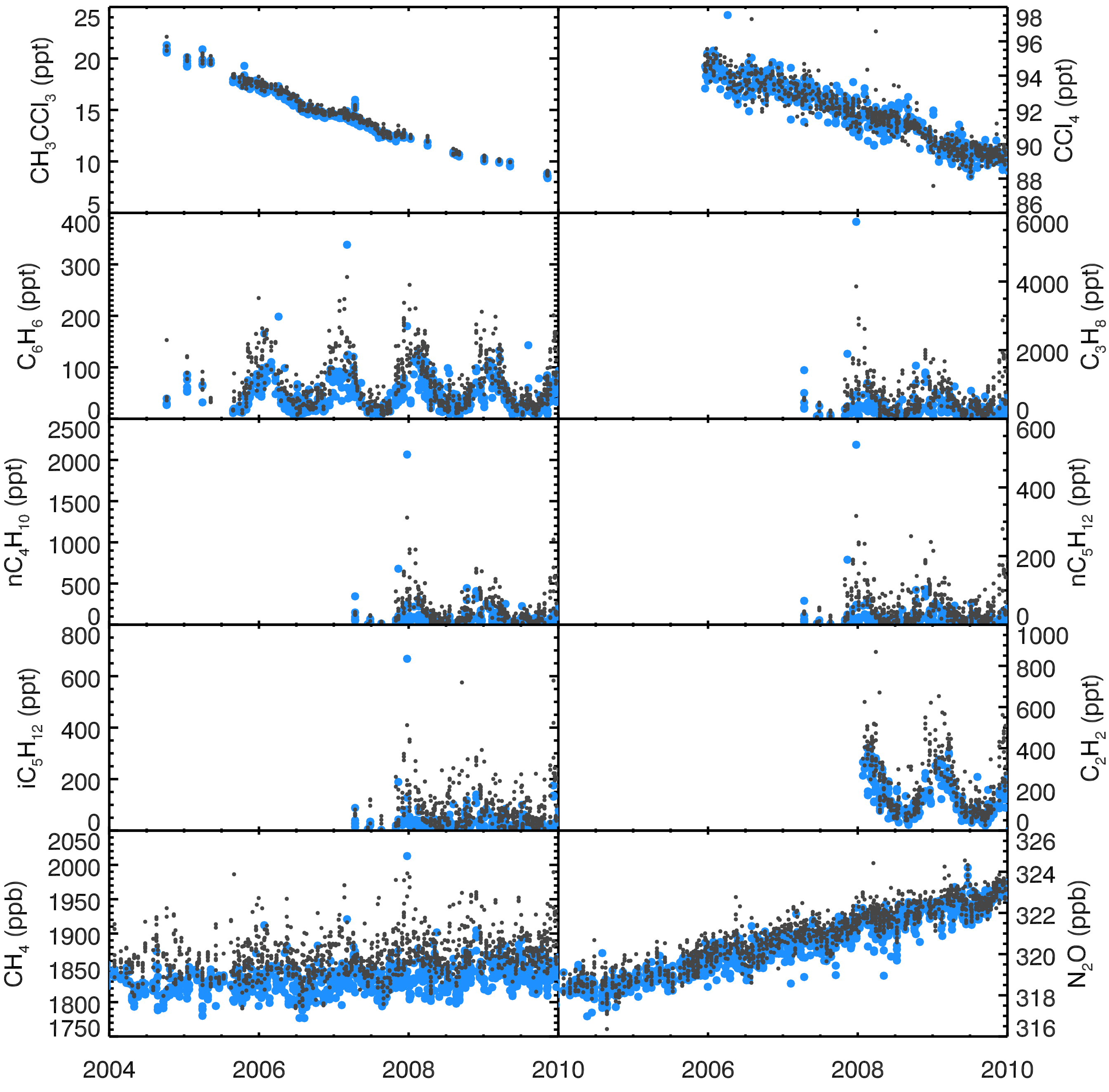

CH_3CCl_3 (ppt)
CCl_4 (ppt)
C_6H_6 (ppt)
C_3H_8 (ppt)
nC_4H_{10} (ppt)
nC_5H_{12} (ppt)
iC_5H_{12} (ppt)
C_2H_2 (ppt)
CH_4 (ppb)
N_2O (ppb)
2004
2006
2008
2010
2006
2008
2010

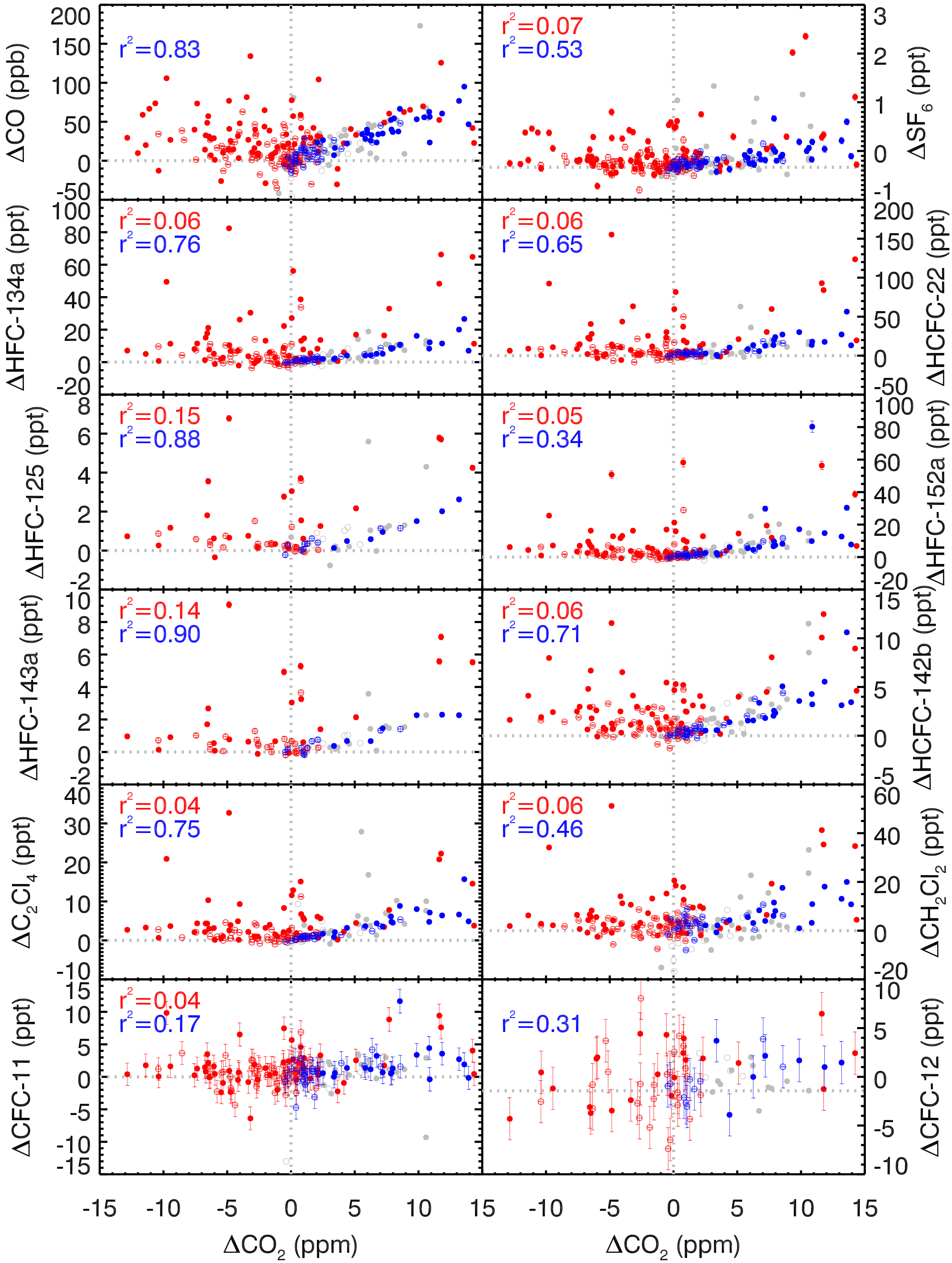

ΔCO (ppb)
r²=0.83
r²=0.07
r²=0.53
ΔSF₆ (ppt)
ΔHFC-134a (ppt)
r²=0.06
r²=0.76
r²=0.06
r²=0.65
ΔHCFC-22 (ppt)
ΔHFC-125 (ppt)
r²=0.15
r²=0.88
r²=0.05
r²=0.34
ΔHFC-152a (ppt)
ΔHFC-143a (ppt)
r²=0.14
r²=0.90
r²=0.06
r²=0.71
ΔHCFC-142b (ppt)
ΔC₂Cl₄ (ppt)
r²=0.04
r²=0.75
r²=0.06
r²=0.46
ΔCH₂Cl₂ (ppt)
ΔCFC-11 (ppt)
r²=0.04
r²=0.17
r²=0.31
ΔCFC-12 (ppt)
ΔCO₂ (ppm)
ΔCO₂ (ppm)

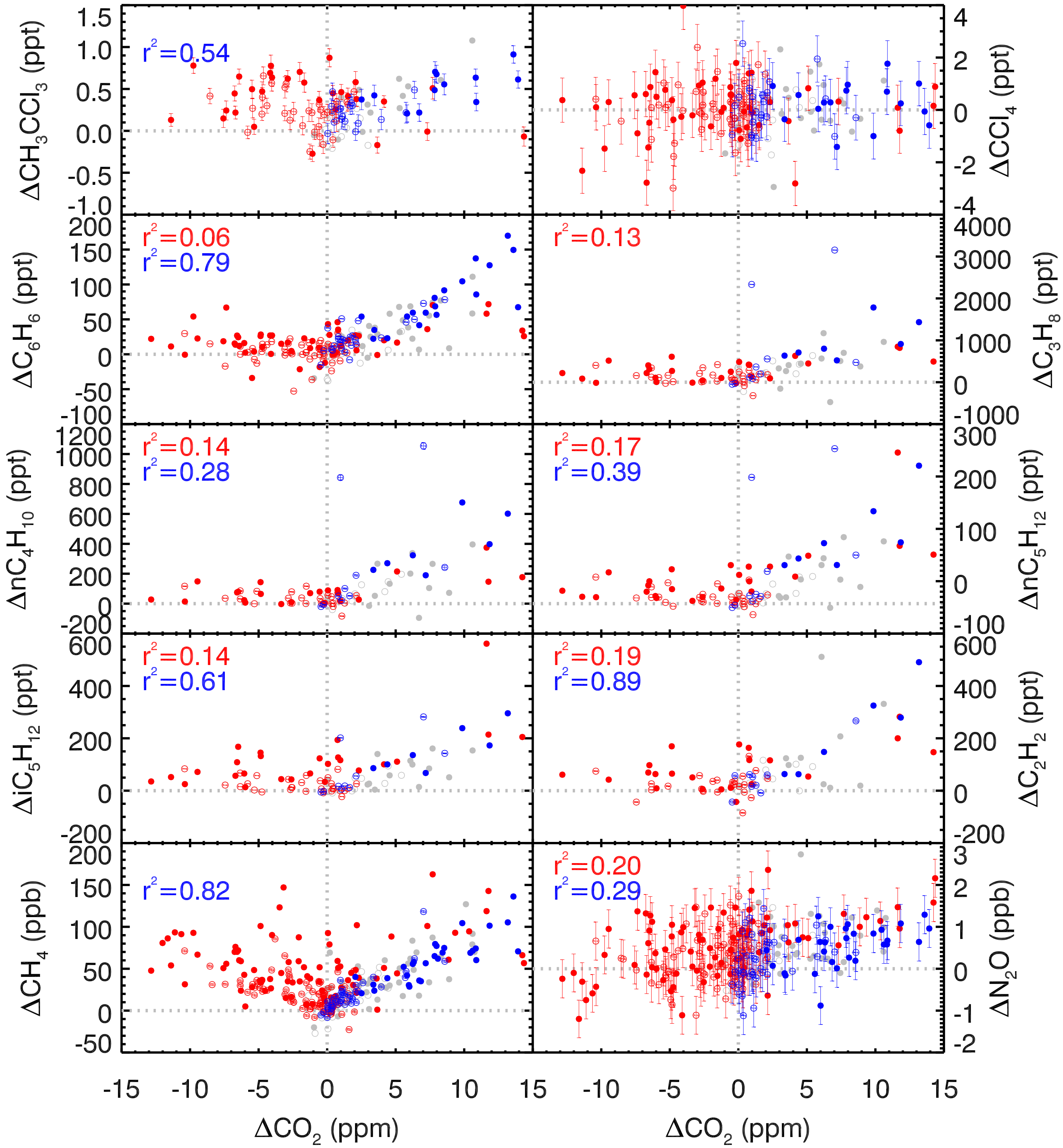

ΔCH3CCl3 (ppt)
ΔCCl4 (ppt)
ΔC6H6 (ppt)
ΔC3H8 (ppt)
ΔnC4H10 (ppt)
ΔnC5H12 (ppt)
ΔiC5H12 (ppt)
ΔC2H2 (ppt)
ΔCH4 (ppb)
ΔN2O (ppb)
ΔCO2 (ppm)
ΔCO2 (ppm)
r²=0.54
r²=0.06
r²=0.79
r²=0.13
r²=0.14
r²=0.28
r²=0.17
r²=0.39
r²=0.14
r²=0.61
r²=0.19
r²=0.89
r²=0.82
r²=0.20
r²=0.29

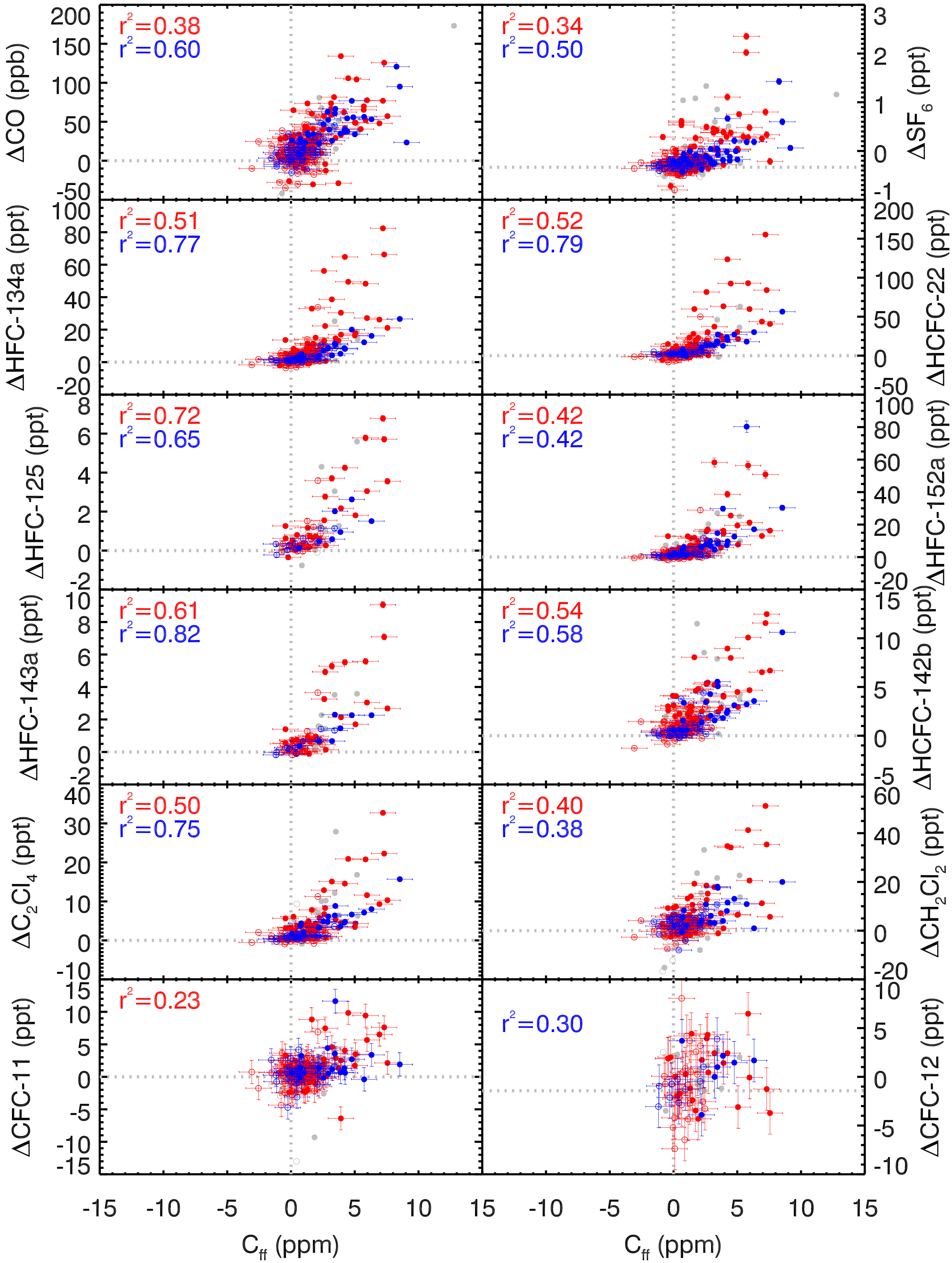

ΔCO (ppb)
ΔSF$_6$ (ppt)
ΔHFC-134a (ppt)
ΔHCFC-22 (ppt)
ΔHFC-125 (ppt)
ΔHFC-152a (ppt)
ΔHFC-143a (ppt)
ΔHCFC-142b (ppt)
ΔC$_2$Cl$_4$ (ppt)
ΔCH$_2$Cl$_2$ (ppt)
ΔCFC-11 (ppt)
ΔCFC-12 (ppt)
r^2=0.38
r^2=0.60
r^2=0.34
r^2=0.50
r^2=0.51
r^2=0.77
r^2=0.52
r^2=0.79
r^2=0.72
r^2=0.65
r^2=0.42
r^2=0.42
r^2=0.61
r^2=0.82
r^2=0.54
r^2=0.58
r^2=0.50
r^2=0.75
r^2=0.40
r^2=0.38
r^2=0.23
r^2=0.30
C_{ff} (ppm)
C_{ff} (ppm)

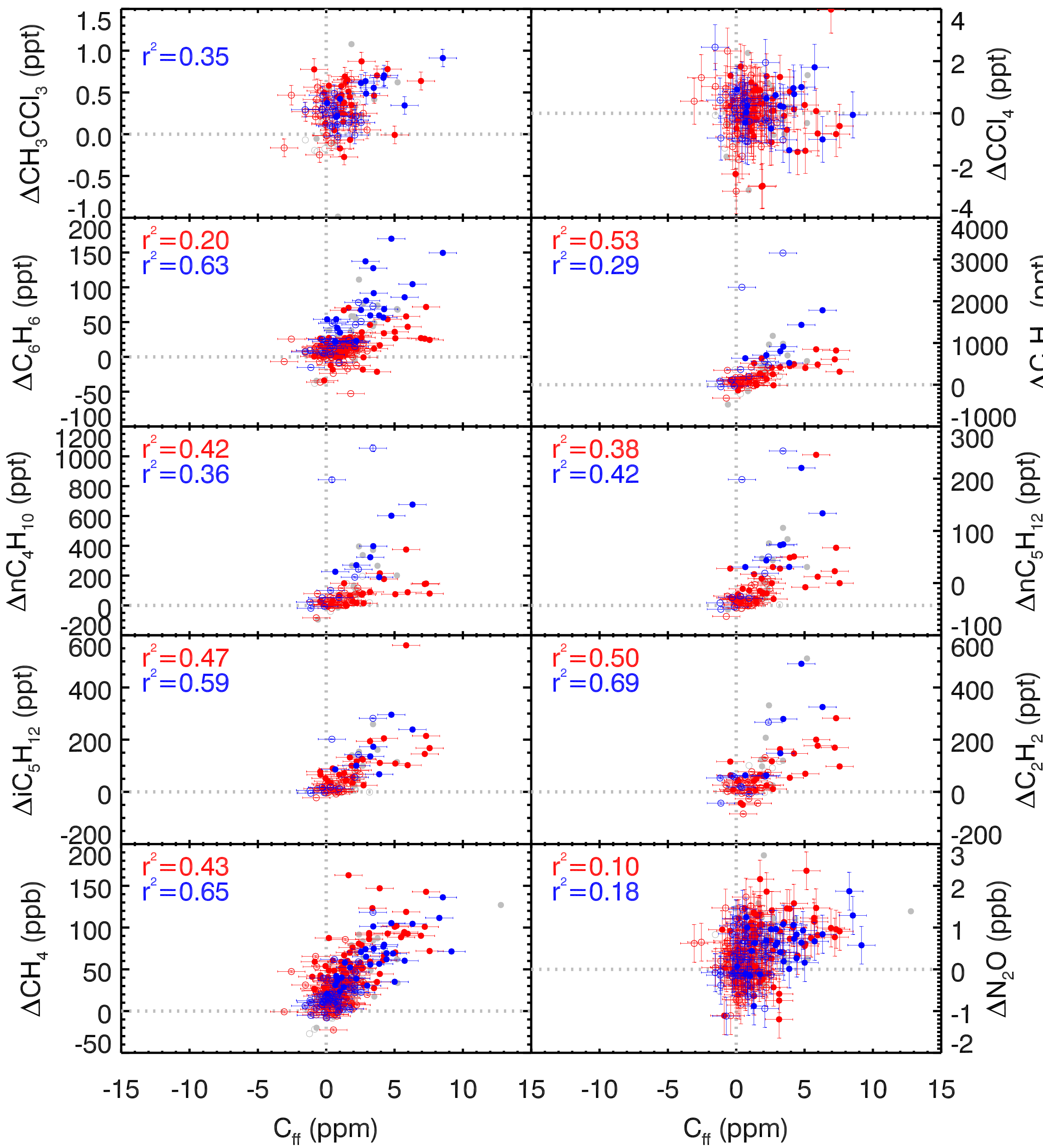

ΔCH3CCl3 (ppt)
r²=0.35
ΔCCl4 (ppt)
ΔC6H6 (ppt)
r²=0.20
r²=0.63
ΔC3H8 (ppt)
r²=0.53
r²=0.29
ΔnC4H10 (ppt)
r²=0.42
r²=0.36
ΔnC5H12 (ppt)
r²=0.38
r²=0.42
ΔiC5H12 (ppt)
r²=0.47
r²=0.59
ΔC2H2 (ppt)
r²=0.50
r²=0.69
ΔCH4 (ppb)
r²=0.43
r²=0.65
ΔN2O (ppb)
r²=0.10
r²=0.18
Cff (ppm)
Cff (ppm)

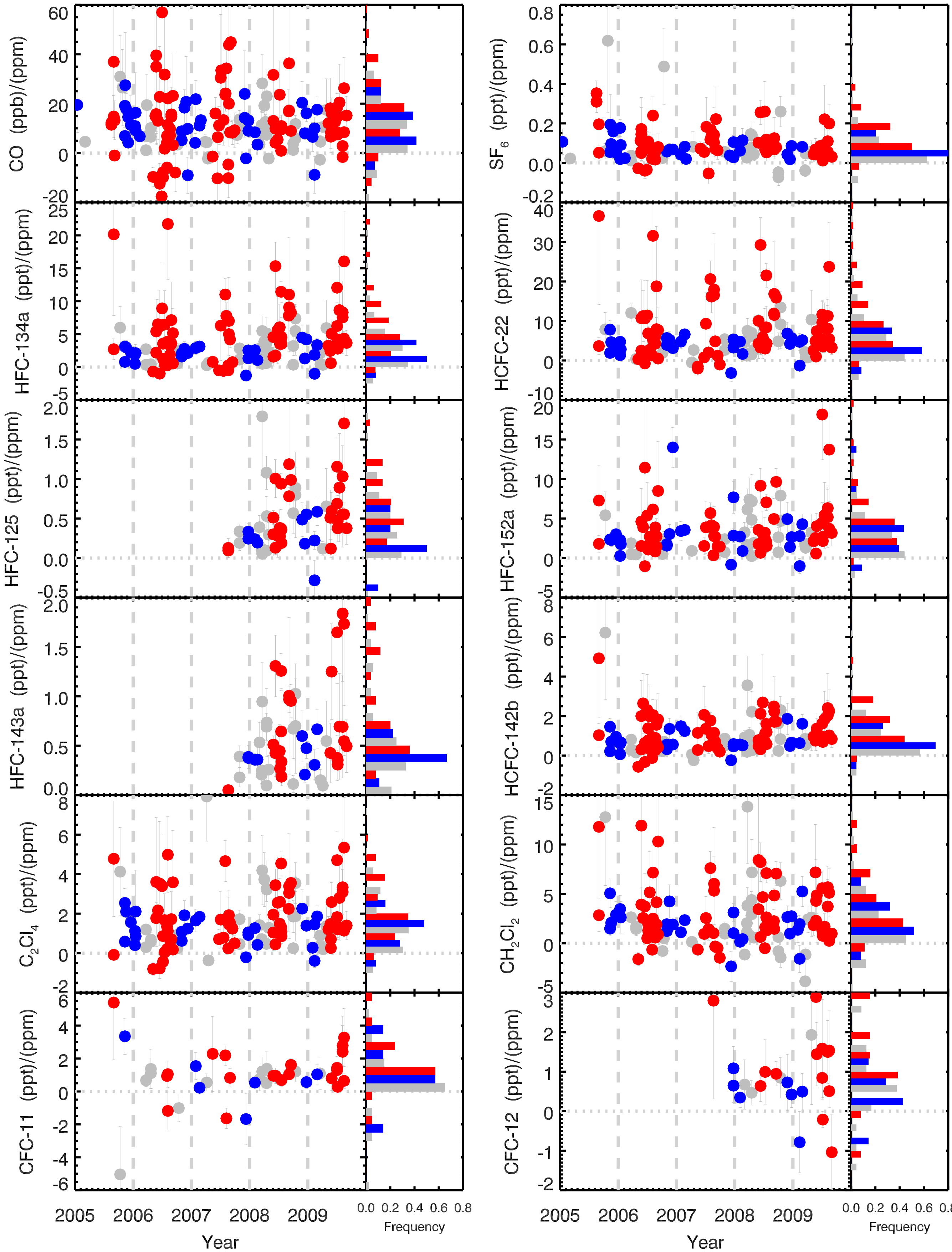

CO (ppb)/(ppm)
HFC-134a (ppt)/(ppm)
HFC-125 (ppt)/(ppm)
HFC-143a (ppt)/(ppm)
C_2Cl_4 (ppt)/(ppm)
CFC-11 (ppt)/(ppm)
SF_6 (ppt)/(ppm)
HCFC-22 (ppt)/(ppm)
HFC-152a (ppt)/(ppm)
HCFC-142b (ppt)/(ppm)
CH_2Cl_2 (ppt)/(ppm)
CFC-12 (ppt)/(ppm)
2005
2006
2007
2008
2009
Year
0.0 0.2 0.4 0.6 0.8
Frequency

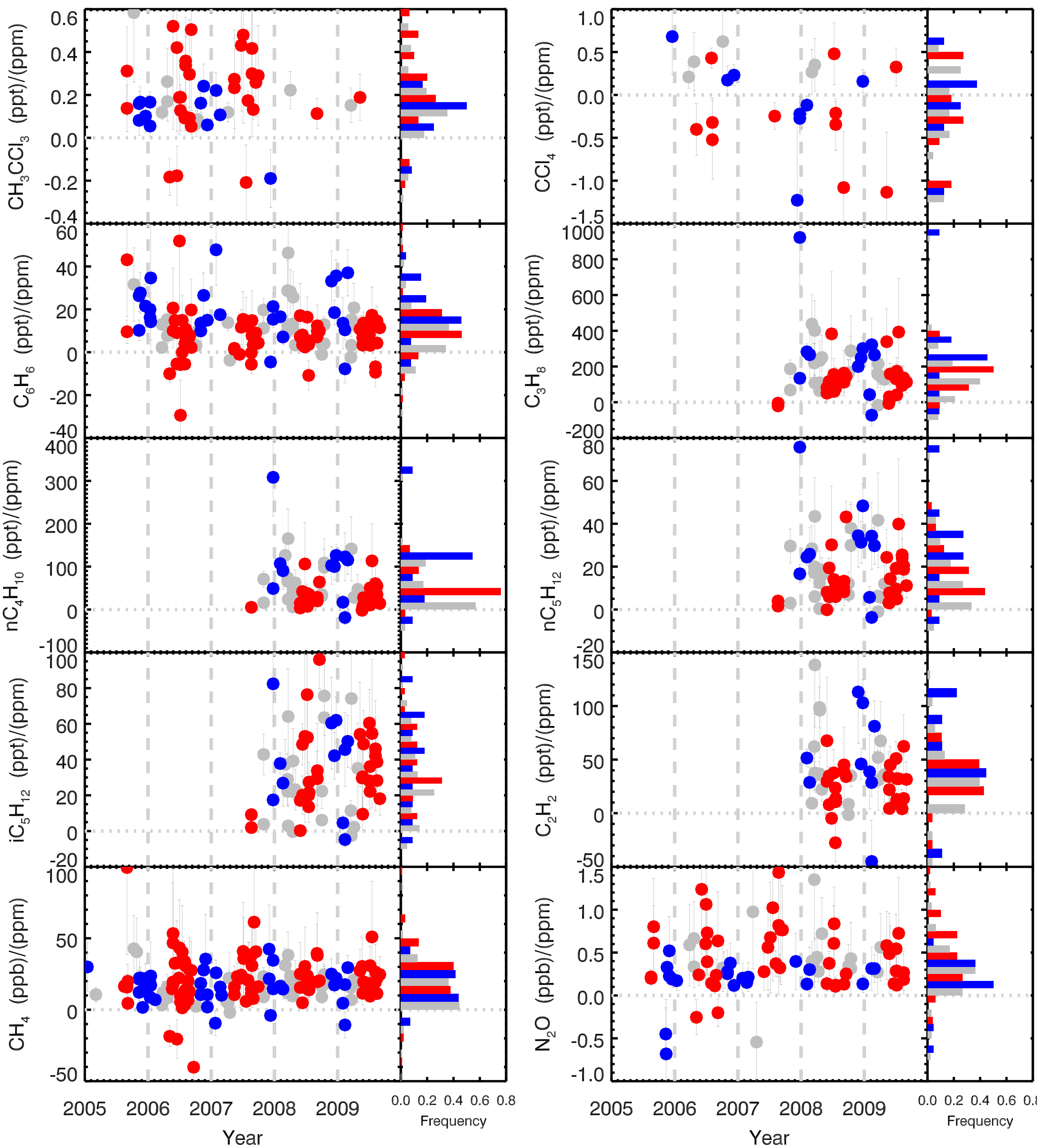

CH_3CCl_3 (ppt)/(ppm)
CCl_4 (ppt)/(ppm)
C_6H_6 (ppt)/(ppm)
C_3H_8 (ppt)/(ppm)
nC_4H_{10} (ppt)/(ppm)
nC_5H_{12} (ppt)/(ppm)
iC_5H_{12} (ppt)/(ppm)
C_2H_2 (ppt)/(ppm)
CH_4 (ppb)/(ppm)
N_2O (ppb)/(ppm)
2005 2006 2007 2008 2009
Year
0.0 0.2 0.4 0.6 0.8
Frequency

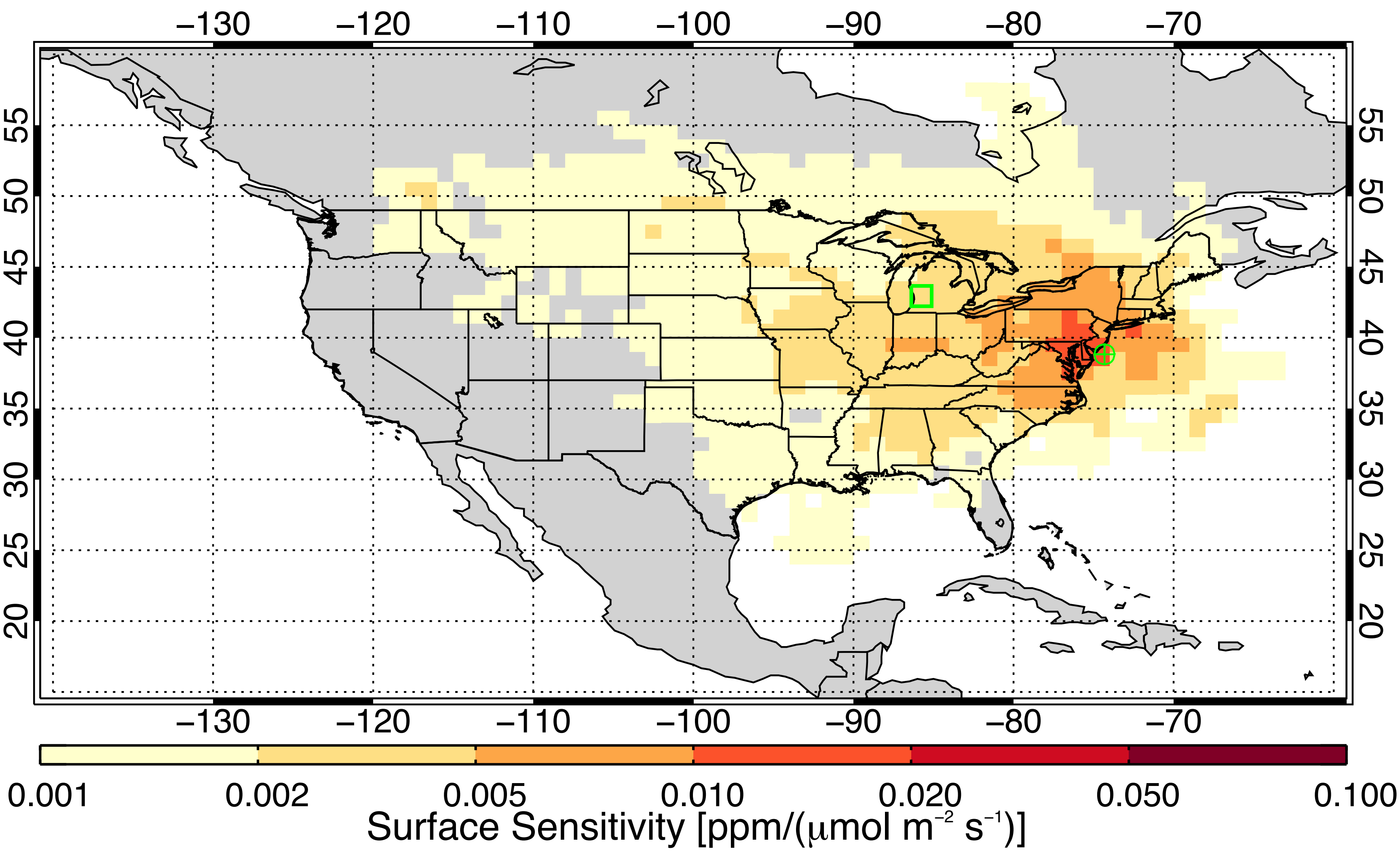

−130
−120
−110
−100
−90
−80
−70
55
50
45
40
35
30
25
20
0.001
0.002
0.005
0.010
0.020
0.050
0.100
Surface Sensitivity [ppm/(μmol m⁻² s⁻¹)]

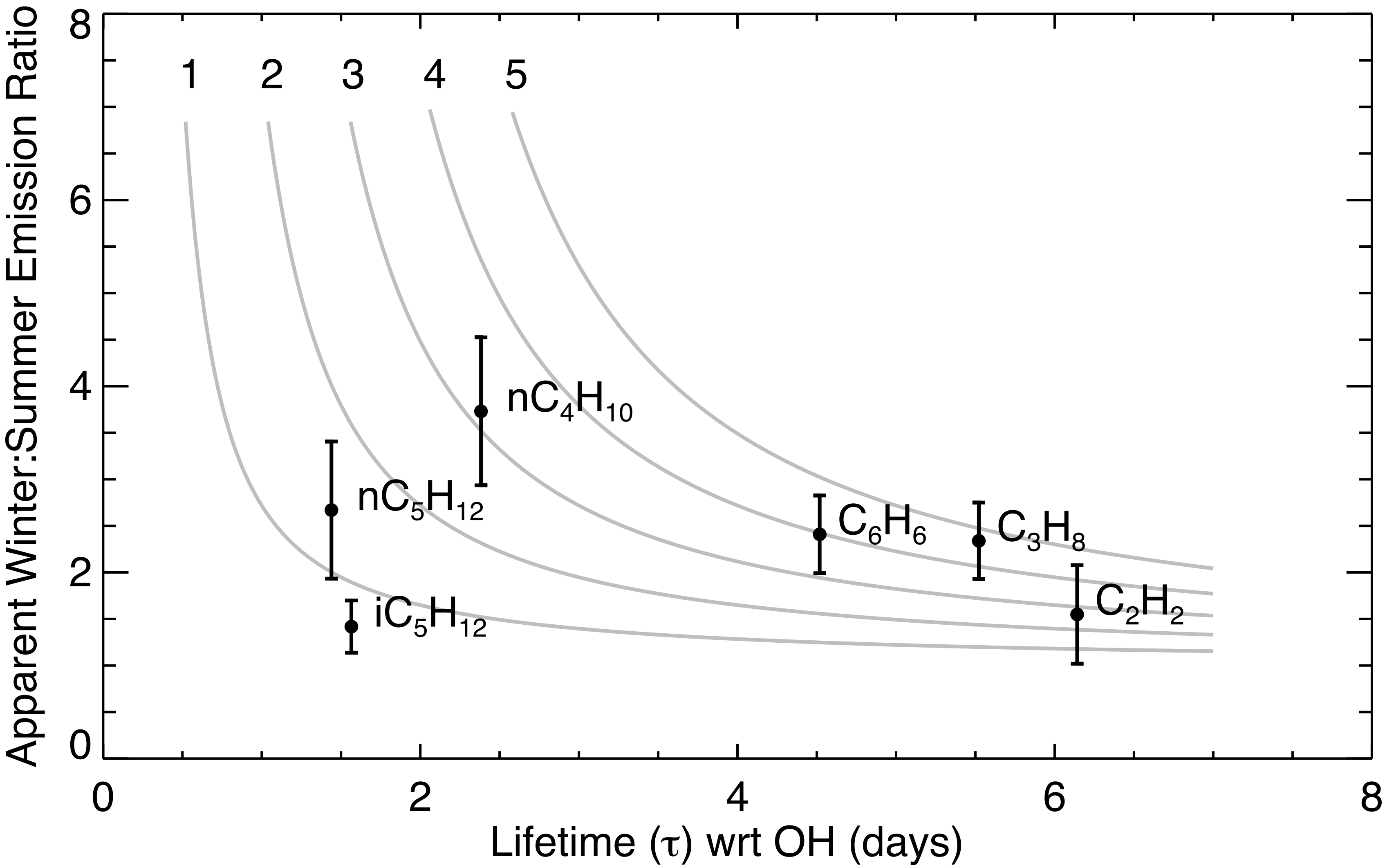

Apparent Winter:Summer Emission Ratio
Lifetime (τ) wrt OH (days)
0
2
4
6
8
1
2
3
4
5
nC4H10
nC5H12
iC5H12
C6H6
C3H8
C2H2

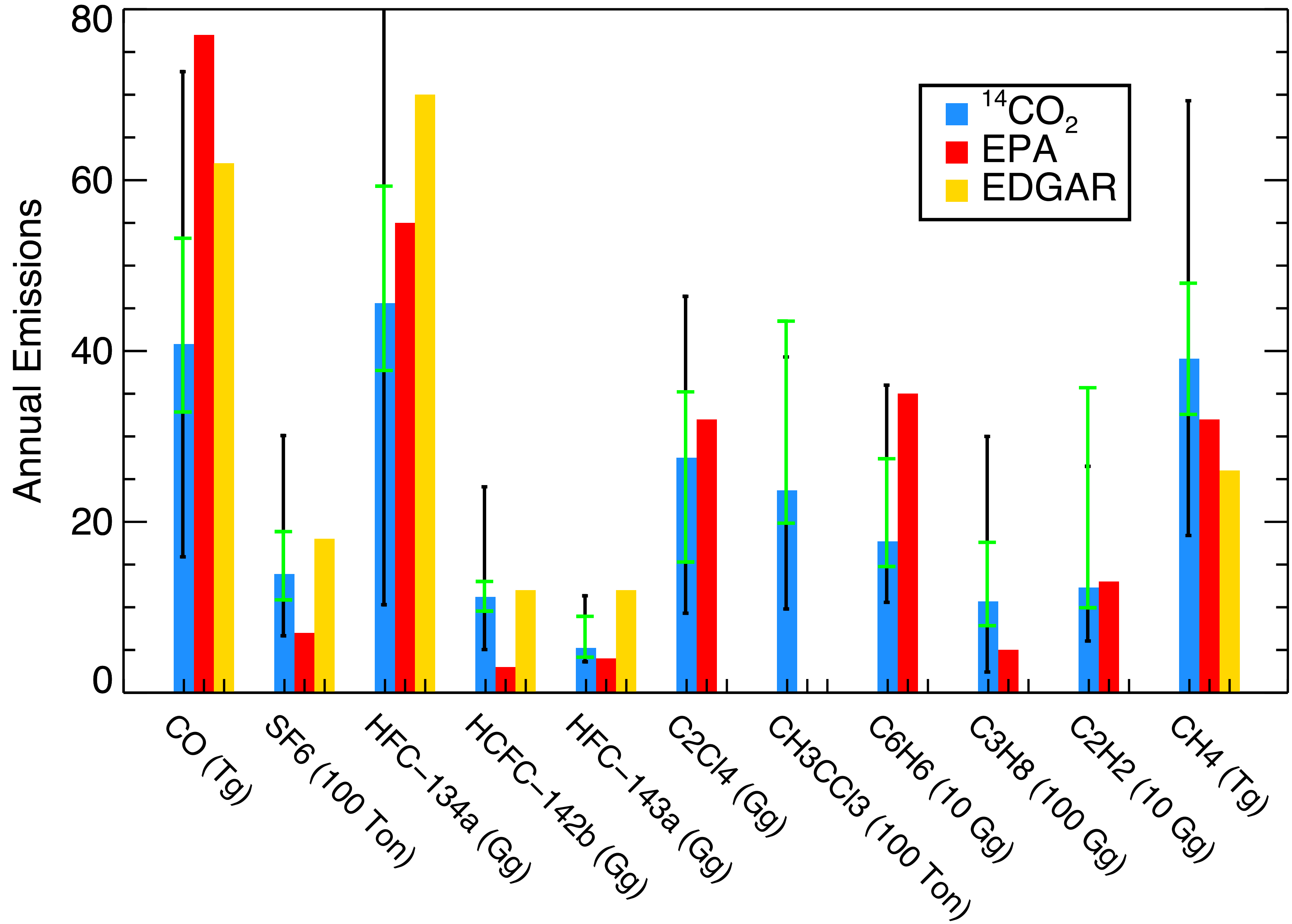

Annual Emissions
0
20
40
60
80
$^{14}CO_2$
EPA
EDGAR
CO (Tg)
SF6 (100 Ton)
HFC−134a (Gg)
HCFC−142b (Gg)
HFC−143a (Gg)
C2Cl4 (Gg)
CH3CCl3 (100 Ton)
C6H6 (10 Gg)
C3H8 (100 Gg)
C2H2 (10 Gg)
CH4 (Tg)

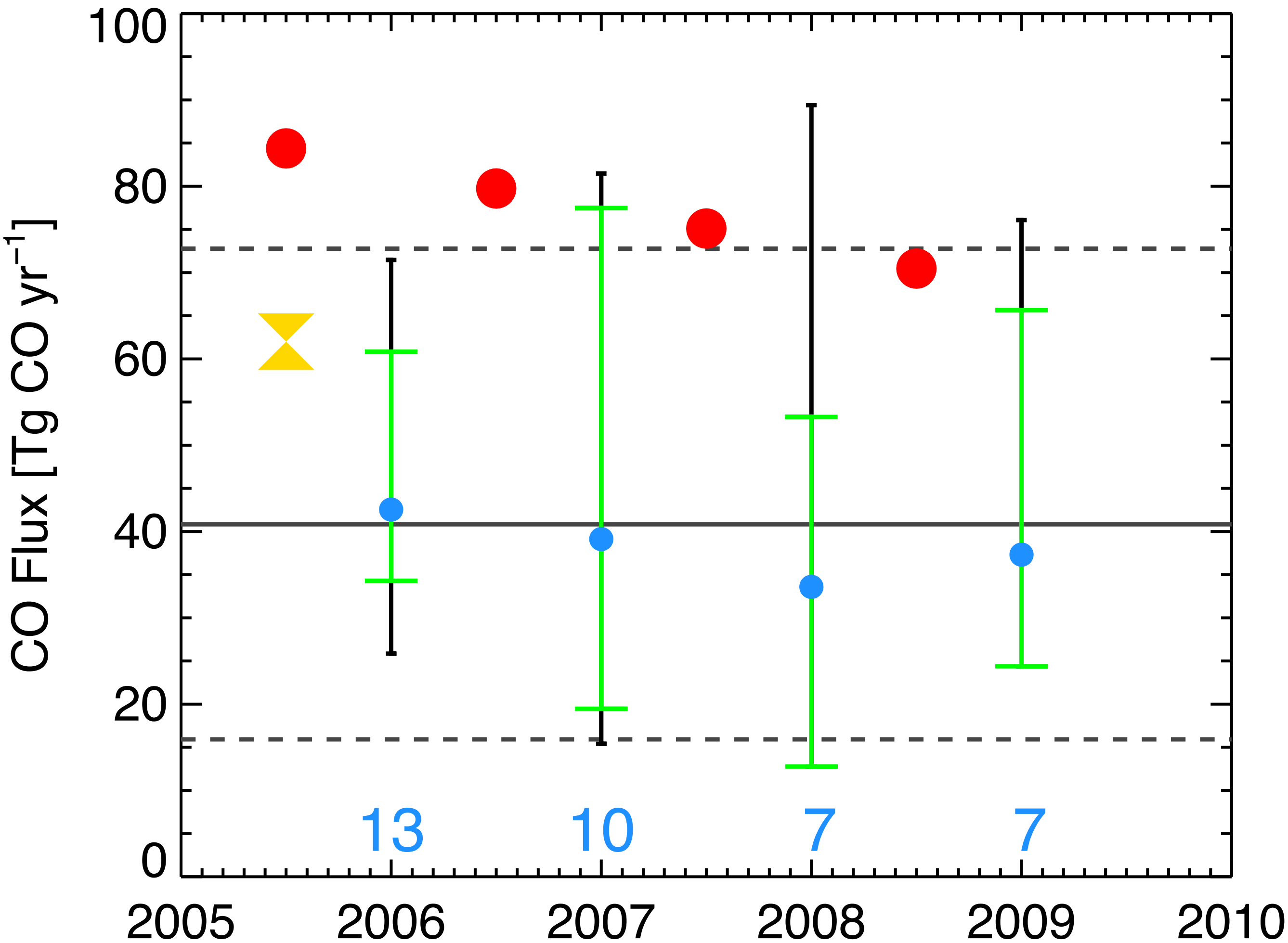

CO Flux [Tg CO yr^{-1}]
100
80
60
40
20
0
13
10
7
7
2005
2006
2007
2008
2009
2010